Physics – Uspekhi **49** (1) 19 – 51 (2006)

REVIEWS OF TOPICAL PROBLEMS

PACS numbers: **33.50. – j**, **33.70. – w**, **78.67. – n**

Blinking fluorescence of single molecules and semiconductor nanocrystals

I S Osad'ko

DOI: 10.1070/PU2006v049n01ABEH002088

Contents

Abstract. **Papers are discussed in which the quantum dynamics of individual molecules and semiconductor nanocrystals is studied from their fluctuating fluorescence. Presented are the fundamental tenets of the theory of photon emission by a single nanoparticle irradiated by continuous laser light. Fluorescence fluctuations which occur only for single nanoparticles are shown to open up entirely new opportunities for investigating nanoparticle quantum dynamics. It is shown how the theory can be harnessed to analyze the fluorescence fluctuations of an individual polymer molecule and a semiconductor nanocrystal and how the corresponding microscopic models can be constructed proceeding from this analysis.**

I S Osad'ko P N Lebedev Physics Institute, Russian Academy of Sciences, Leninskii prosp. 53, 119991 Moscow, Russian Federation
Tel. (7-495) 132 68 34
E-mail: osadko@sci.lebedev.ru

Received 11 October 2004, revised 4 April 2005
Uspekhi Fizicheskikh Nauk **176** (1) 23 – 57 (2006)
Translated by E N Ragozin; edited by A Radzig

1. Introduction

The invention and wide use of microscopes with atomic resolution (scanning tunnel microscopes, and atomic-force microscopes) or with subatomic resolution (near-field microscopes) have fostered the rapid broadening of investigations of individual nanoparticles of various natures. The term nanoparticle will be used in reference to a molecule, a semiconductor nanocrystal, or a metal nanoparticle containing several hundred or thousand atoms interacting with each other, which may be treated as a quasimolecule.

Luminescent methods are most effective in the investigation of single nanoparticle dynamics. Fluorescence photons emitted by a single nanoparticle that experiences continuous excitation by laser light or the tunnel current of a scanning tunnel microscope are the source of information about the local dynamics of the nanoparticle and its local environment. The greatest wealth of material acquired to date relates to single-molecule spectroscopy (SMS).

The spectroscopy of single molecules might be associated with the spectroscopy of a molecule that does not interact with the rest, i.e., with the spectroscopy of a strongly rarefied molecular gas. This idea is an utter fallacy, because SMS is the spectroscopy of molecules introduced into a solid matrix

(polymer, glass, or crystal) whose natural optical absorption domain is separated from the optical impurity absorption domain by a substantial energy interval. It is evident that intermolecular interaction has a significant effect on the optical band of the impurity molecule, and it is precisely this intermolecular interaction that is the main subject of investigation in SMS which offers two fundamental advantages over the spectroscopy of molecular ensembles.

The first advantage. In disordered matrices like polymer or glass, the local environment is different for various individual impurity molecules. This results in the inhomogeneous broadening of the optical bands and the loss of information about the local properties of individual impurity centers, when we record the photons absorbed or emitted by all molecules from the ensemble of impurity centers. When we record the photons absorbed or emitted by only one molecule, such a photon sequence is a source of information about the specific individual molecule and its local environment. SMS, which provides us with information on the interaction between an individual impurity center and its local environment, therefore offers an enormous advantage over the spectroscopy of molecular ensembles, in which this information remains concealed.

The second advantage. The spectroscopy of single molecules permits investigation of the local dynamics of an impurity center, i.e., of a molecule interacting with the nearest environment. This dynamics manifests itself in the absorption coefficient being time-dependent. However, extracting this temporal dependence from experimental data is complicated by the fact that these data in SMS are fluctuating in nature.

Investigation of fluctuations underlies SMS. Any event in the microworld is accidental and takes place with a certain probability. In a molecular ensemble, random events add up and allow us to deal with the probability of an event, which, on the other hand, we can calculate by quantum-mechanical techniques. That is why no fundamental problems arise when comparing the theoretical and experimental data: the measured probability can be compared with the calculated one. By contrast, every single event being measured in SMS comprises a fluctuation. For instance, a change in the local environment of an impurity molecule, occurring during its irradiation and affecting its absorption frequency, will have the effect that the quantum transition in the molecular environment will manifest itself in a jump in the resonance frequency of the molecular line. In other words, a fluctuation of the absorption coefficient of precisely this individual molecule will take place. SMS experimental data are immanently fluctuating in nature. Therefore, in SMS there arises the problem of statistical processing of fluctuations for the purpose of deriving the probability which may be compared with the probability calculated in the framework of the theoretical model.

However, two new problems emerge in the theory of SMS spectroscopy: *the problem of calculating the absorption coefficient dependent on the measurement time*, and *the problem of calculating fluctuations*. The calculated and measured fluctuations may also be compared with each other, although on a qualitative basis only. The form of fluctuations depends strongly on the signal accumulation time which is hard to vary in experiment but is quite easy to vary in theory. That is why the theory permits investigation of the effect of the signal accumulation time on the character of fluctuations in SMS. This capability of the theory is of prime importance, because it enables 'interpretation' of the experimentally found fluctuations. By fluctuation 'interpretation' is meant the formulation of a theoretical model capable of reproducing fluctuations similar to those obtained in experiment. Examples of such an 'interpretation' of fluctuations will be provided in Sections 12 and 13. The features of the procedure of comparing experimental data and theoretical calculations in SMS are schematically diagrammed in Fig. 1. The links indicated with slanting arrows in Fig. 1, which reveal the specific SMS features, will be discussed in detail in Section 9.

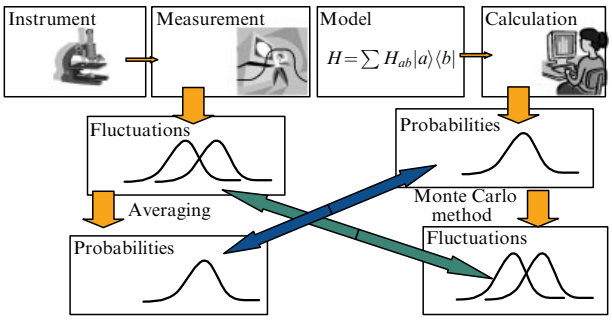

Figure 1. Diagrammatic representation of the comparison between experiment and theory in the spectroscopy of single nanoobjects.

The investigation of single nanoparticles began with a study of single atoms in the gaseous phase [1 – 3], which preceded investigations of single molecules in solid matrices. The achievements in this field are reviewed in Ref. [4]. The spectroscopy of single molecules emerged only about fifteen years ago [5, 6] and initially developed as the low-temperature spectroscopy of a limited class of single impurity molecules dissolved in a paraterphenyl crystal or polymers. The achievements of the first years are reflected in review articles [7 – 10] and the monograph [11].

However, beginning in the mid-1990s there occurred a rapid expansion of the class of molecules studied by SMS techniques [12 – 22] and a start was made on the investigation of single quantum dots in semiconductors [23 – 34]. In this works, single molecules and sometimes quantum dots were investigated at room temperature, which is of extraordinary importance from the standpoint of the practical use of the findings of these papers. This review is concerned with a discussion of experimental data acquired during the last five years and their theoretical interpretation.

2. Principles of experimental spectroscopic methods for studying single nanoparticles

The technique for measuring fluorescence excitation spectra is the central SMS research method. Indeed, the light absorption technique is inefficient in the study of a single molecule, because it is difficult to observe the disappearance of one photon from the huge number of photons of sample-irradiating laser light. It is by far more expedient to investigate absorption by observing fluorescence. That is why measurements of the total fluorescence as a function of the exciting laser frequency are made. This method is equivalent to the measurement of the absorption coefficient and relies on the premise that the fluorescence intensity of a molecule is proportional to the intensity of light it absorbs. Since the fluorescence spectrum always moves up in wavelengths with relation to the absorption spectrum, then by

placing a light filter behind the sample it is possible to practically completely cut off the photons of exciting light, making it much easier to detect the fluorescence photons shifted relative to them in frequency. Furthermore, the signal-to-noise ratio turns out to be significantly greater than in the light absorption method.

Two development stages are clearly recognizable in the short history of SMS. At the first stage, which lasted till approximately the mid-1990s, pentacene molecules and several other molecules of the aromatic series were investigated as single molecules. These molecules share the common property of large absorption coefficient and high quantum yield of fluorescence. Paraterphenyl crystals, in which these molecules are easily dissolved without forming aggregates or polymers were selected for a solid matrix.

Low-temperature experiments. It is well known that the optical band of an impurity center consists of a phononless line (PLL) and a phonon wing (PW) which corresponds to electron–phonon transitions. Owing to the weakness of electron–phonon interaction in organic matrices, the impurity band intensity is concentrated mainly in the PLL whose width becomes smaller as the temperature is lowered. At temperatures of 4.2 K and below, the PLL width is equal to several hundred megahertz.

Since laser light can be focused onto a spot no smaller than the light wavelength squared in area, i.e., on the order of 0.2–0.3 μm^2, the laser spot will contain dozens of impurity molecules even for a concentration of 10^{-9} mol l^{-1}. However, since these molecules will find themselves in a different local environment, their phononless transition frequencies in the polymer matrix will be spread over an interval on the order of the inhomogeneous distribution function width equal to ≈ 100 cm^{-1} or 3×10^4 GHz in the polymer, i.e., over an interval which exceeds the PLL width by many orders of magnitude. By selecting a laser excitation frequency equal to the PLL frequency of some individual molecule, we will therefore excite the fluorescence of only this particular molecule. Despite the irradiation, other molecules are not excited because their PLL frequencies do not coincide with the laser radiation frequency.

If we wanted to study the time dependence of some physical characteristics of a molecular ensemble with the aid of fluorescence photons, we would evidently have to resort to pulsed excitation of the sample so as to transfer the ensemble to an unsteady state. In this case, too, the spectroscopy of single molecules gave us a surprise: it enables the study of the local dynamics of an impurity center, i.e., the time dependence of its characteristics employing a continuous excitation source. Furthermore, a continuous excitation source is more advantageous than the pulsed one because it furnishes the possibility of accumulating more fluorescence photons within a given time.

Even the first experiments on single molecules revealed that the optical line corresponding to the first electronic transition may execute jumps in frequency [35, 36]. The line jumps, as was established later, are related to the effect of positional changes of the solvent atoms in the neighborhood of an impurity molecule, i.e., to the effect of so-called two-level systems (TLSs). More than thirty years ago Anderson et al. [37] and Phillips [38] introduced the concept of the glass TLSs to which there correspond spontaneous changes in the equilibrium positions of atoms or groups of atoms in glass. These changes were described in the framework of the TLS model. The TLS excitation energies occupy the frequency range from zero to ≈ 30 cm^{-1}. The TLS concept was later extended to polymers and other disordered solids as well. The spontaneous change in the equilibrium atomic position represents a quantum jump from one TLS state to the other. The local environment of the impurity molecule affects its electronic excitation energy, i.e., the position of the molecular spectral line. That is why the quantum jump from one TLS state to the other would lead to a frequency jump of the spectral line of the impurity molecule.

When the exciting laser frequency is scanned through a spectral range which includes the optical line of a given individual molecule, the spectral line will be measured at different spectral positions during different laser scans, i.e., it will execute jumps. The duration of laser scanning typically ranges between one and several seconds [36, 39, 40]. Consequently, the spectral line jumps also occur on the time scale of seconds. Since the line jumps are caused by the jumps of an atom entering the local environment, these infrequent jumps are an indication that the TLS transitions from one quantum state to the other are tunnel type transitions.

Room-temperature experiments. A substantial broadening of the class of molecules and the passage to room-temperature research became possible through the use of confocal microscopes in SMS. Recourse to confocal microscopy marked the onset of the second stage of SMS development. The amount of work on SMS increased steeply and the research subjects came to be more diversified. Considerable interest was attracted to the newly opened possibility of investigating single polyatomic dye molecules [14] and molecules of the biological class like polymer molecules [12, 17, 21], dendrimer molecules [19, 22], light-harvesting antennas of photosynthesis centers [18], protein molecules [15], enzymes [16], and even single DNA molecules with built-in chromophores [13]. Since biological molecules function at room temperature, it is vital to investigate such single objects at room temperature. An advantage of the confocal microscope over conventional luminescence microscope consists in the cut-off of stray luminescence light from the elements of the sample, which are not related directly to the molecules under study. It is evident that one cannot 'see' through the confocal microscope a spot smaller than λ^2, where λ is the fluorescence light wavelength. Consequently, the solution with the molecules investigated should contain no bigger than one molecule over such an area, which is really attainable for a concentration of less than 10^{-10} mol l^{-1}.

As regards the fluorescence of single molecules themselves, it can be observed with a conventional luminescence microscope. Simple estimates suggest that this is possible. Indeed, assuming a dye absorption cross section $\sigma = 10^{-16}$ cm^2, a laser power $I = 100$ W cm^{-2}, and a photon energy $E = 3 \times 10^{-19}$ J, we find that the number of absorption events per second is $I\sigma/E = 30{,}000$ s^{-1}. On putting the quantum yield of fluorescence equal to 0.5, the light grasp by the lens equal to 0.125, and the transmittance of all remaining optics to 0.5, we arrive at an efficiency of visually recorded light of 3%, which corresponds to about $30{,}000 \times 0.03 \approx 1000$ photons per 1 s. This photon flux exceeds the visual threshold by a factor of about 20.

As a rule, the optical bands of complex organic molecules are structureless at room temperature. This is evident from Fig. 2 which portrays the absorption and fluorescence bands of the poly(p-phenylene vinylene) (PPV) and poly(p-pyridine vinylene) (PPyV) copolymer measured

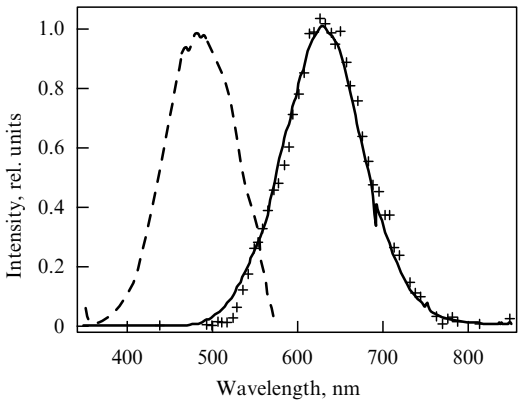

Figure 2. Absorption band (dashed curve) and fluorescence band (solid curve) of the bulk polymer. Crosses show the fluorescence band of a single PPV – PPyV polymer molecule [12].

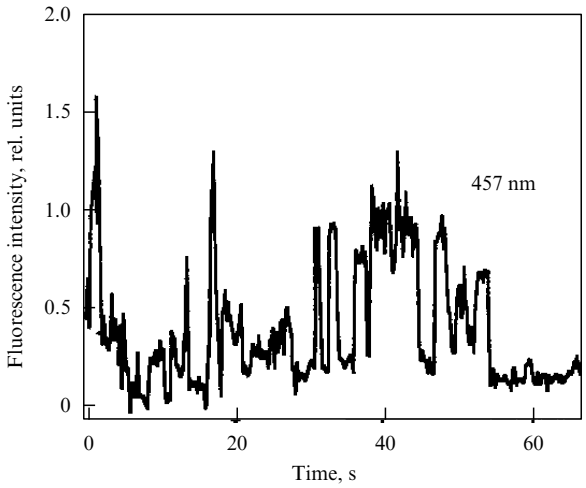

Figure 3. Temporal behavior of the fluorescence (quantum intensity trajectory) of a single PPV – PPyV polymer molecule excited by cw radiation with $\lambda = 457$ nm [12]. The fluorescence signal accumulation time was equal to 0.1 s.

at room temperature [12]. The solid curve corresponds to the fluorescence band of an ensemble of the polymer molecules, and the crosses show the fluorescence band of a single polymer molecule.

From the fact that the fluorescence band of a single molecule practically coincides with the fluorescence band of an ensemble of molecules it follows that the inhomogeneous broadening arising from the spread in electronic excitation frequency is, under these conditions, significantly smaller than the homogeneous broadening caused by electron – phonon interaction. Consequently, the methods of selective spectroscopy, which eliminate inhomogeneous broadening and narrow the optical bands at low temperatures, are powerless in this case. There are no ways of narrowing, with the use of selective spectroscopy techniques, the band width and making it smaller than the homogeneous width which is large in this case. The physical information about a molecule, extractable from this broad band of Gaussian shape, is extremely limited, and therefore spectral methods for the investigation of molecules are ineffective at room temperature. This situation is encountered in the investigation of any complex organic molecule at room temperature. Employing SMS affords a decisive breakthrough in this important area.

The fundamental difference between the fluorescence of a single polymer molecule and the fluorescence of an ensemble manifests itself not in spectral radiation characteristics (the fluorescence bands are practically coincident), but in the temporal behavior of the fluorescence. The fluorescence intensity of an ensemble of polymer molecules is time-independent on a dozens-of-seconds scale, while the fluorescence intensity of a single polymer molecule fluctuates, as shown in Fig. 3.

It is precisely these intensity fluctuations of a broad fluorescence band that permit studying the dynamics of energy transfer and other intramolecular processes in a single polymer molecule at room temperature. And it is precisely these fluctuations that are the source of information about the dynamics of a complex molecule, which is considered at length in Section 12. In the molecular ensemble, the fluorescence fluctuations vanish owing to the averaging of the fluctuations of many molecules. In parallel with this averaging, an important source of information closes in the molecular ensemble. It is evident that the central point in the fluorescence theory of a single molecule (a nanoparticle) is the calculation of fluorescence photon emission probability for the molecule under continuous irradiation by laser light. The basics of this calculation are outlined in Sections 3 – 5.

3. Different ways of counting fluorescence photons

An atom under continuous light irradiation emits one fluorescence photon at random instants of time. The location of these random instants on the time scale reflects the quantum dynamics of the atom as discussed below in this review. A quantum yield of fluorescence of less than unity, an incomplete collection of the fluorescence light, and not total counting efficiency of the photomultiplier (PM) will have the effect that an emitted photon will not correspond to every absorbed photon and that the notions 'photon emission event' and 'photon recording event' will be distinct. The above-listed factors are not representative of quantum atomic dynamics and, as shown by Mandel and Wolf [41], are responsible for relatively trivial corrections to the formulas containing the photon counting rate. That is why they will not be considered in this review.

The question of the probability of observing N fluorescence photons emitted by a single atom under continuous light irradiation over a time interval T was first discussed by Mandel [42]. The author of that work employed the following formula for the probability of observing N fluorescence photons on a time interval T [41 – 44]:

$$w(N,T) = \left\langle T : \frac{1}{N!} \left[\int_t^{t+T} \mathrm{d}x\, \hat{I}(x) \right]^N \exp\left[- \int_t^{t+T} \mathrm{d}x\, \hat{I}(x) \right] : \right\rangle . \quad (1)$$

Here, the normal and chronologically ordered product of intensity operators $\hat{I}$ appears under the sign $\langle\ \rangle$ of quantum-statistical averaging, and t is the current time.

Formula (1) may equally be applied to an atomic ensemble and a single atom. Suppose an experiment involves counting the number of acts $n_N(T,t)$ that N fluorescence photons are emitted during a time interval T for a total observation time t. The probability of this event is defined by

the formula

$$w_N(T) = \lim_{t\to\infty} \frac{n_N(T,t)}{n_0(T,t) + \sum_{N=1}^{\infty} n_N(T,t)} . \qquad (2)$$

It is precisely the experimentally obtained probability $w_N(T)$ that can be compared with the theoretical probability (1), i.e., $w_N(T)$ should be equal to the probability $w(N,T)$ calculated by formula (1) for a given physical model. The calculation of the photon probability distribution by formula (1) for the fluorescence of atomic ensembles can be found in monograph [41].

Paradoxically enough, the probability calculation by formula (1) for a single atom is a more intricate task than for an atomic ensemble. This supposedly is the reason why the computation for a single atom has not been performed so far. Mandel [42] replaced this calculation with a simpler problem of calculating the distribution function moments. Mandel came up with the idea of estimating, with the use of these moments, the degree of deviation of the photon distribution from the Poisson distribution by the parameter

$$Q(T) = \frac{\langle N^{(2)}(T)\rangle - \langle N(T)\rangle^2}{\langle N(T)\rangle} , \qquad (3)$$

where $\langle N^{(2)}(T)\rangle$ is the second factorial moment, and $\langle N(T)\rangle$ is the average number of photons on an interval T. With formulas (1) and (2), the Mandel parameter takes on the form

$$Q(T) = \langle I\rangle \left[\frac{2}{T}\int_0^T \mathrm{d}x \int_0^x \mathrm{d}y\, g^{(2)}(y) - T \right] , \qquad (4)$$

where $g^{(2)}(t)$ is the autocorrelation function of fluctuating fluorescence, as discussed in Section 7.2. Formula (4) expressing the Mandel parameter in terms of the autocorrelation function which may be found experimentally, turned out to be highly convenient for a practical estimation of the degree of photon distribution deviation from the Poisson one and was employed for the analysis of specific situations [45–47]. For the Poisson distribution, the Mandel parameter $Q(T)$ is equal to zero. For a distribution narrower than the Poisson one, i.e., for a sub-Poisson distribution, $Q(T) < 0$; for a broader (super-Poisson) distribution, $Q(T) > 0$. Formula (4) is commonly employed to estimate the degree to which the photon distribution in the luminescence of single atoms and molecules deviates from the Poisson distribution.

It is pertinent to note that formula (4) contains a sort of incorrectness, because it makes use of the relationship $\langle N(T)\rangle = \langle I\rangle T$ which does not take into account the so-called photon antibunching, as discussed at the end of Section 5. As will be seen in Section 6, it is precisely the photon antibunching that is responsible for deviations from the Poisson photon distribution function, and it should therefore be taken into account in the calculation of the average number of photons as well.

Considered in Mandel's approach to the computation of the photon distribution function is the radiation field itself. However, the statistics of photons emitted by a single atom is amenable to study from the dynamics of atomic excited-to-ground state transitions, because every atomic transition to the electronic ground state is accompanied by the emission of a fluorescence photon. This approach to the single-atom research is more fruitful than that employed by Mandel because it allows a direct theoretical evaluation of the probabilities $w(N,T)$, which will be shown in Sections 4 and 5. But first we consider two possible ways of fluorescence photon counting in the conditions of continuous excitation of a single atom.

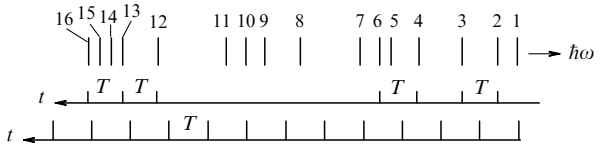

Figure 4. Photon sequence emitted by an atom under continuous light excitation.

Let a two-level atom continuously irradiated by a laser emit fluorescence photons at random instants of time. Vertical dashes in Fig. 4 indicate the fluorescence photons emitted by this atom (which are numbered for convenience of discussion). Mandel's formula (1) corresponds to that way of photon counting in which the time scale is divided into uniform intervals, as shown on the lower time scale in Fig. 4, and which involves counting the number of photons emitted during each interval. In this case, the onset of a time interval is in no way related to the instant of photon emission. During some of the time intervals, photons are not emitted at all, as shown in Fig. 4.

However, in the investigation of luminescence from a single atom, another way of fluorescence photon counting is possible. This way is attractive in that it allows not only the derivation of the theoretical formula for the fluorescence photon distribution function, which will be seen to differ from formula (1), but the calculation of this formula as well. We will enlarge on this approach.

Let a fluorescence photon be emitted at some zero point in time. This point is taken as the beginning of an interval. Let another photon be emitted at the expiration of a time interval T. This instant is taken as the end of the interval. Therefore, only the intervals of length T with at least two photons are considered in this case. Shown on the upper time scale in Fig. 4 are four such intervals. The following two variants are possible.

(1) Between the emission of the photon, opening the interval T, and the emission of the photon, closing this interval, no other photons were emitted. Such are the intervals between the emission of photons 2 and 3 as well as 12 and 13, shown in Fig. 4. The probability of second photon emission is correlated. It is precisely this situation which is described by the *start–stop correlator* considered below in Section 4. This mode was named the mode of sequentially emitted photons by Kim et al. [48].

(2) In between the emissions of two photons, separated by a given interval T, additional photons may be emitted, which will be referred to as *intermediate*. For instance, in between the emission events with photons 4 and 6, which are separated by the interval T, one intermediate photon 5 was emitted, while two intermediate photons 14 and 15 were emitted in between the emissions of photons 13 and 16. By counting all photon pairs separated by the interval T, we thereby measure, no matter how many intermediate photons were emitted on the interval T, the *full two-photon correlator*, as discussed in Section 5.

By drawing on the approach developed in the author's papers [11, 49], we now will derive the mathematical expression for the probability of detecting different numbers of intermediate photons on the interval T.

4. Two-photon 'start – stop' correlator

We begin with a consideration of the time intervals containing no intermediate photons. Let us assume that an atom emits a fluorescence photon at a point in time taken to be zero. This signifies that the atom occupies, at the zero instant of time, the ground electronic state with a probability equal to unity. The probability that the atom will emit a second photon at the point in time t can be found from the equations for probability amplitudes:

$$\dot{G}_{lm}(t) = -\mathrm{i}\omega_l G_{lm}(t) - \frac{\mathrm{i}}{\hbar}\sum_s V_{ls} G_{sm}(t)\,, \tag{5}$$

where the probability amplitudes are defined by the relationship $G_{lm}(t) = -\mathrm{i}\langle l\,|\exp\left(-\mathrm{i}(H_0+V)t/\hbar\right)|m\rangle$, H_0 is the Hamiltonian of the atom – field system with the eigenvalues $\hbar\omega_l$, and V_{ls} are the matrix elements of the atom – light interaction operator in the basis of the eigenfunctions of the H_0 operator. In the resonance approximation, sometimes also referred to as the rotating wave approximation, the interaction operator links the following states of the atom – field system between themselves:

$$\left|\begin{matrix}0\\n\end{matrix}\right\rangle \leftrightarrow \left|\begin{matrix}1\\n-1\end{matrix}\right\rangle \leftrightarrow \left|\begin{matrix}0\\n-1,\,k\end{matrix}\right\rangle \leftrightarrow \left|\begin{matrix}1\\n-2,\,k\end{matrix}\right\rangle \leftrightarrow \ldots\,. \tag{6}$$

Here, 0 and 1 denote the ground and excited atomic states, n is the number of photons in the laser mode, and k is the index of the quantum state of the spontaneous fluorescence photon, which also includes the photon polarization. We introduce the following notation for the matrix elements [11]:

$$\begin{aligned}
&\frac{1}{\hbar}\left\langle\begin{matrix}0\\n\end{matrix}\right|V\left|\begin{matrix}1\\n-1\end{matrix}\right\rangle = \mathrm{i}\lambda_0\sqrt{n+1} \approx \mathrm{i}\chi\,,\\
&\frac{1}{\hbar}\left\langle\begin{matrix}1\\n-1\end{matrix}\right|V\left|\begin{matrix}0\\n-1,\,k\end{matrix}\right\rangle = -\mathrm{i}\lambda_k\,,
\end{aligned} \tag{7}$$

where $\chi = \mathbf{Ed}/\hbar$ is the Rabi frequency expressible in terms of the electric field vector $\mathbf{E}$ of the light wave and the dipole moment $\mathbf{d}$ of the atomic transition. In the basis of states (6), the system of equations (5) takes on the form

$$\begin{aligned}
&\dot{G}^0_n(t) = -\mathrm{i}\omega^0_n G^0_n + \chi G^1_{n-1}\,,\\
&\dot{G}^1_{n-1}(t) = -\mathrm{i}(\omega^0_n + \Delta)\,G^1_{n-1}(t) - \chi G^0_n(t) - \sum_k \lambda_k G^0_{n-1k}(t)\,,\\
&\dot{G}^0_{n-1k}(t) = -\mathrm{i}(\omega^0_n + \Delta_k)\,G^0_{n-1k}(t) + \lambda_k G^1_{n-1} + \underline{\chi G^1_{n-2k}}\,,\\
&\qquad\qquad \ldots\,.
\end{aligned} \tag{8}$$

The system of equations (8) is infinite. Here, the subscript m of the initial state is omitted from the amplitudes and use is made of the following notation: $\Delta = \Omega - \omega_0$, and $\Delta_k = \omega_k - \omega_0$, where Ω, ω_0, and ω_k are the respective frequencies of electronic excitation, the laser mode, and the spontaneously emitted photon.

We now calculate the Fourier transforms of the right- and left-hand sides of Eqns (8). We employ the formula

$$(\dot{G})_\omega = -G(t=0) - \mathrm{i}(\omega + \mathrm{i}0)\,G(\omega)\,,$$

put $\omega^0_n = 0$, and take into account the initial condition $G^0_n(0) = -\mathrm{i}$ to arrive at the following system of equations for the Fourier components:

$$\begin{aligned}
&G_0(\omega) = \frac{1}{\omega + \mathrm{i}0} + \frac{\mathrm{i}}{\omega + \mathrm{i}0}\,\chi G_1(\omega)\,,\\
&G_1(\omega) = \frac{-\mathrm{i}}{\omega - \Delta + \mathrm{i}0}\left[\chi G_1(\omega) + \sum_k \lambda_k G_k(\omega)\right],\\
&G_k(\omega) = \frac{\mathrm{i}}{\omega - \Delta_k + \mathrm{i}0}\left[\lambda_k G_1(\omega) + \underline{\chi G_{1k}(\omega)}\right],\\
&\qquad\qquad \ldots\,.
\end{aligned} \tag{9}$$

Here, we simplified in an obvious manner the indices on the probability amplitudes.

In the solution of the system of equations (9) we can represent the amplitude G_1 in the form of a continued fraction

$$G_1 = \cfrac{-\mathrm{i}\chi G_0}{\omega - \Delta - \sum_k \cfrac{\lambda_k^2}{\omega - \Delta_k - \cfrac{\chi^2}{\underline{\omega - \Delta - \Delta_k - \sum_{k'} \cfrac{\lambda_{k'}^2}{\ldots}}}}}\,, \tag{10}$$

in which large quantities χ^2, being corresponded to a great number of laser mode photons, alternate with small matrix elements λ_k^2. A small matrix element 'dumps out' the effect of the large quantity that appears lower in the fraction and permits us to neglect the contribution to G_1 made by the underlined fraction. We may therefore discard it. This approximation corresponds to discarding the terms underlined in the systems of equations (8) and (9), i.e., to breaking the infinite chain of equations for the probability amplitudes. In this approximation, we can derive, in view of the system of equations (8) and its complex conjugate system, the following probability conservation law

$$\frac{\mathrm{d}}{\mathrm{d}t}\left(W_0 + W_1 + \sum_k W_k\right) = 0\,, \tag{11}$$

where $W_0 = |G_0|^2$, $W_1 = |G_1|^2$, and $W_k = |G_k|^2$ are the probabilities that an atom is found, respectively, in the ground and excited states and again in the ground state upon emission of the fluorescence photon k. The temporal behavior of the probabilities appearing in expression (11) is as follows. At the zero point in time, $W_0 = 1$, and $W_1 = \sum_k W_k = 0$. Since the laser light continues to irradiate the atom, W_0 will tend to zero, W_1 will initially increase and then tend to zero, while the probability $\sum_k W_k$ that the fluorescence photon has been emitted will turn to unity for large values of time, which is physically justified. In Section 5 we will show that the probability of photon emission during the interval $(t, t+\mathrm{d}t)$ tends to zero. Consequently, despite the break in the infinite chain of equations, the temporal behavior of approximate amplitudes appears physically reasonable. The truncated system of equations (8) does not describe the emission of the third and subsequent photons. In Section 5 we will consider the equations for such processes as well.

In view of the third equation of system (8), we obtain the relationship

$$\frac{\mathrm{d}}{\mathrm{d}t}\sum_k W_k = \sum_k \lambda_k\left(G_k(t)\,G_1^*(t) + G_k^*(t)\,G_1(t)\right). \tag{12}$$

On the other hand, we find, in view of the third equation of system (9), the relation for the Fourier components:

$$\sum_k \lambda_k G_k(\omega) = \mathrm{i} \sum_k \frac{\lambda_k^2}{\omega - \Delta_k + \mathrm{i}0}\, G_1(\omega)\,. \tag{13}$$

Calculation of the sum on the right-hand side of Eqn (13) will yield a real quantity and an imaginary one. The real part of the sum may, considering the renormalization procedure possible for electromagnetic interaction, always be included in the corresponding resonance frequency. We therefore consider only the imaginary quantity which describes the decay of the excited electronic state. Its calculation was set forth in appendix Π1 to the book [11], where it was shown that the right-hand side of Eqn (13) can be represented in the form

$$\sum_k \lambda_k G_k(\omega) = \frac{1}{2T_1}\, G_1(\omega)\,. \tag{14}$$

Here, T_1 is the lifetime of the excited atomic level. Clearly, a similar relationship is valid for the time components as well:

$$\sum_k \lambda_k G_k(t) = \frac{1}{2T_1}\, G_1(t)\,. \tag{15}$$

Using this relationship, we can bring equation (12) to the form

$$\mathrm{d} \sum_k W_k(t) = \frac{W_1(t)}{T_1}\, \mathrm{d}t\,. \tag{16}$$

Since $\sum_k W_k(t)$ defines the probability that a fluorescence photon is emitted by the *point* in time t, the function

$$s(t) = \frac{W_1(t)}{T_1} \tag{17}$$

defines the probability density for the fluorescence photon detection *on the interval* $(t, t + \mathrm{d}t)$ which is counted from the zero point in time — the instant of emission of the first photon. This function, which describes the correlation between the second photon emission time and the first photon emission time, tends to zero with increasing t and was therefore termed the start – stop correlator [11, 49].

In view of relationship (15), we can rearrange the second equation of system (8), with the result that the system assumes the form

$$\begin{aligned} \dot{G}_0 &= \chi G_1\,, \\ \dot{G}_1 &= -\mathrm{i}\left(\Delta - \frac{\mathrm{i}}{2T_1}\right) G_1 - \chi G_0\,. \end{aligned} \tag{18}$$

We introduce the following notation for the elements of the density matrix:

$$\begin{aligned} &\left|G_0(t)\right|^2 = W_0\,, \qquad \left|G_1(t)\right|^2 = W_1\,, \\ &G_0(t)\, G_1^*(t) = W_{01}\,, \qquad G_1(t)\, G_0^*(t) = W_{10}\,. \end{aligned} \tag{19}$$

Then, the system of equations (18) and its complex conjugate system allow us to arrive at the following system of equations for the elements of the density matrix:

$$\begin{aligned} \dot{W}_{10} &= -\mathrm{i}\left(\Delta - \frac{\mathrm{i}}{2T_1}\right) W_{10} + \chi(W_0 - W_1)\,, \\ \dot{W}_{01} &= \mathrm{i}\left(\Delta + \frac{\mathrm{i}}{2T_1}\right) W_{01} + \chi(W_0 - W_1)\,, \\ \dot{W}_1 &= -\chi(W_{10} - W_{01}) - \frac{W_1}{T_1}\,, \\ \dot{W}_0 &= \chi(W_{10} - W_{01})\,. \end{aligned} \tag{20}$$

The system of equations (20) contains transition probabilities which are measured in start – stop experiments on single molecules [50] and is different from the Bloch equation in that the term W_1/T_1 is missing from the fourth equation. From system (20), there follows the relationship

$$\dot{W}_0 + \dot{W}_1 = -\frac{W_1}{T_1}\,. \tag{21}$$

On the other hand, from the probability conservation law described by Eqn (11) it follows that

$$\dot{W}_0 + \dot{W}_1 = -\frac{\mathrm{d}}{\mathrm{d}t} \sum_k W_k\,. \tag{22}$$

With the aid of the last two equations we arrive again at formulas (16) and (17), which define the start – stop correlator. The probability $W_1(t)$ in the start – stop correlator should be calculated from Eqns (20) subject to the initial condition $W_0(0) = 1$.

We emphasize that when the time t significantly exceeds T_1 the probability $s(t)$ of detecting the second photon of the start – stop pair *at the point in time t* tends to zero, even though the probability $\sum_k W_k(t)$ tends to unity, i.e., the start – stop correlator tends to zero rather rapidly. Such a correlator is inadequate for the investigation of the slow dynamics of an impurity center in a polymer or glass, which occurs over periods significantly exceeding the time T_1. That is why in practice advantage is taken of a different experimental scheme whereby measurements are made of the so-called full two-photon correlator. In this case, *any pair* of photons separated by a given time interval t, without regard for the number of intermediate fluorescence photons emitted between the emission events of the photons that open and close this interval, is detected. We will derive below the expression for the full two-photon correlator.

5. Full two-photon correlator

Functions (6) demonstrate that the complete Fock space of the atom – field system may be partitioned into the Fock subspaces characterized by a certain number N of spontaneously emitted fluorescence photons. An example of the Fock subspace with $N = 0$ is provided by the first two functions in scheme (6), with $N = 1$ being the second two functions, etc. When an atom experiences continuous excitation by light, there occur transitions between different Fock subspaces. Figure 5 illustrates transitions of this sort: induced, which occur with a rate k, and spontaneous, which occur with a rate $1/T_1$. The scheme shows that the atom converts the laser field photons to fluorescence photons; $\rho_0^{(N)}$, and $\rho_1^{(N)}$ describe the probabilities that the atom is found,

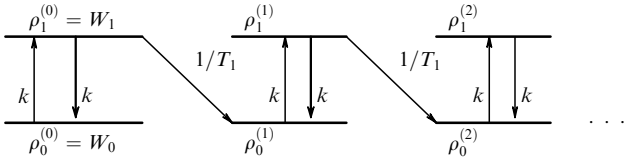

Figure 5. Radiative transitions between the states containing different numbers of fluorescence photons.

respectively, in the ground state and in the excited state with spontaneous emission of N fluorescence photons by the atom, i.e., in the Nth Fock subspace. For a continuously operating pump laser, the laser photons are constantly converted to atomic fluorescence photons.

First, let us consider a simplified version of the theory and describe the dynamics of such a system by balance equations. For the probabilities depicted in Fig. 5, we can write out the following system of balance equations:

$$\begin{aligned}
&\dot{W}_1 = -\left(k + \frac{1}{T_1}\right) W_1 + kW_0\,,\\
&\dot{W}_0 = kW_1 - kW_0\,,\\
&\dot{\rho}_1^{(1)} = -\left(k + \frac{1}{T_1}\right) \rho_1^{(1)} + k\rho_0^{(1)}\,,\\
&\dot{\rho}_0^{(1)} = k\rho_1^{(1)} - k\rho_0^{(1)} + \frac{W_1}{T_1}\,,\\
&\dot{\rho}_1^{(2)} = -\left(k + \frac{1}{T_1}\right) \rho_1^{(2)} + k\rho_0^{(2)}\,,\\
&\dot{\rho}_0^{(2)} = k\rho_1^{(2)} - k\rho_0^{(2)} + \frac{\rho_1^{(1)}}{T_1}\,,\\
&\qquad\cdots\\
&\dot{\rho}_1^{(N)} = -\left(k + \frac{1}{T_1}\right) \rho_1^{(N)} + k\rho_0^{(N)}\,,\\
&\dot{\rho}_0^{(N)} = k\rho_1^{(N)} - k\rho_0^{(N)} + \frac{\rho_1^{(N-1)}}{T_1}\,,\\
&\qquad\cdots .
\end{aligned} \tag{23}$$

Here, the first two equations describe the dynamics of the system without intermediate photons, i.e., the start – stop mode. The next two equations for the functions $\rho^{(1)}$ describe the dynamics of the system with one intermediate photon, and so on. We introduce the functions

$$\rho_0(t) = \sum_{N=0}^{\infty} \rho_0^{(N)}(t)\,, \qquad \rho_1(t) = \sum_{N=0}^{\infty} \rho_1^{(N)}(t) \tag{24}$$

for the probability that the atom is found in the ground and excited states for an arbitrary number of emitted fluorescence photons. If we sum separately the odd and even equations of system (23), we will find that the new transition probabilities satisfy the following balance equations

$$\begin{aligned}
&\dot{\rho}_1 = -\left(k + \frac{1}{T_1}\right) \rho_1 + k\rho_0\,,\\
&\dot{\rho}_0 = \left(k + \frac{1}{T_1}\right) \rho_1 - k\rho_0\,.
\end{aligned} \tag{25}$$

We take the Fourier transform of the functions W_0 and W_1 in the first two Eqns (23), as well as in the system of equations (25), and solve the resultant algebraic equations. Since the determinants of these two systems for the Fourier components obey the relationship $\det_W = \det_\rho + k/T_1$, it is easy to verify that their solutions are related in the following way:

$$\rho_1(\omega) = W_1(\omega) + \frac{1}{T_1}\, W_1(\omega)\, \rho_1(\omega)\,. \tag{26}$$

We pass on to the time components in relationship (26) to obtain the equation

$$\rho_1(t) = W_1(t) + \int_0^t \frac{\mathrm{d}x}{T_1}\, W_1(t-x)\, \rho_1(x)\,, \tag{27}$$

which couples both probabilities. The last equation can be solved by the iterative method, and we arrive at the following formulas

$$\rho_1(t) = W_1(t) + \sum_{N=1}^{\infty} \rho_1^{(N)}(t)\,, \tag{28}$$

where

$$\begin{aligned}
\rho_1^{(N)}(t) = &\int_0^t \frac{\mathrm{d}t_1}{T_1} \int_0^{t_1} \frac{\mathrm{d}t_2}{T_1}\\
&\cdots \int_0^{t_{N-1}} \frac{\mathrm{d}t_N}{T_1}\, W_1(t-t_1)\, W_1(t-t_2)\\
&\cdots W_1(t_{N-1}-t_N) W_1(t_N)\,.
\end{aligned} \tag{29}$$

We divide both sides of formula (28) by $\rho_1(t)$ to obtain the equation

$$1 = w_0(t) + \sum_{N=1}^{\infty} w_N(t)\,, \tag{30}$$

whose right-hand side may be considered as the sum of probabilities, where

$$w_0(t) = \frac{W_1(t)}{\rho_1(t)}\,, \qquad w_N(t) = \frac{\rho_1^{(N)}(t)}{\rho_1(t)} \tag{31}$$

define the respective probabilities of observing an interval of duration t without intermediate photons and with N intermediate photons. From Eqns (23) it follows that $W_1(t)$ tends to zero for $t > T_1$. On the other hand, from Eqns (25) it follows that $\rho_1(\infty) \neq 0$. That is why the probability $w_0(t)$ of detecting an interval without intermediate photons tends to zero with increasing t. The formula for $w_0(t)$ may be rewritten as

$$w_0(t) = \frac{W_1(t)}{T_1}\, \frac{T_1}{\rho_1(t)} = \frac{s(t)}{p(t)}\,, \tag{32}$$

where $p(t) = \rho_1(t)/T_1$ may be termed the full two-photon correlator. It defines the probability of recording a photon on the interval $(t, t + \mathrm{d}t)$ with the proviso that an arbitrary number of intermediate photons could be emitted on the interval $(0, t)$. We divide both sides of Eqn (27) by T_1 to find the relation between the start – stop correlator and the full correlator.

In the derivation of formulas (27) – (30) advantage was taken of the balance equations (23) and (25), which do not include the effect of phase relaxation occuring with a rate $1/T_2$. However, a more rigorous treatment carried out in Refs [11, 49, 51 – 54] shows that the inclusion of phase relaxation gives rise to the following equations for the elements of the density matrix corresponding to the quantum

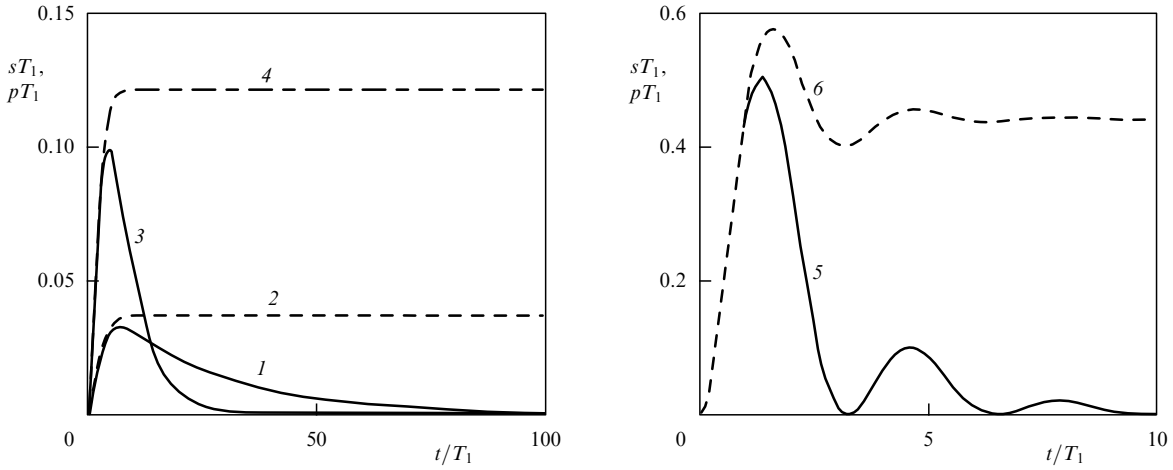

Figure 6. Start–stop correlator (curves *1*, *3*, *5*) and full two-photon correlator (curves *2*, *4*, *6*) as functions of the time delay for different pump intensities: $\chi T_1 = 0.2$ (curves *1*, *2*), 0.3 (curves *3*, *4*), and 1.0 (curves *5*, *6*).

state of the atom–field system with N fluorescence photons, instead of the equations for W_0, W_1, ρ_0, and ρ_1:

$$\begin{aligned}
\dot\rho_{10}^{(N)} &= -\mathrm{i}\left(\Delta - \frac{\mathrm{i}}{2T_1}\right)\rho_{10}^{(N)} + \chi\left(\rho_{11}^{(N)} - \rho_{00}^{(N)}\right), \\
\dot\rho_{01}^{(N)} &= \left(\dot\rho_{10}^{(N)}\right)^*, \\
\dot\rho_{11}^{(N)} &= -\chi\left(\rho_{10}^{(N)} + \rho_{01}^{(N)}\right) - \frac{1}{T_1}\rho_{11}^{(N)}, \\
\dot\rho_{00}^{(N)} &= \chi\left(\rho_{10}^{(N)} + \rho_{01}^{(N)}\right) + \frac{1}{T_1}\rho_{11}^{(N-1)}.
\end{aligned} \tag{33}$$

Here, $\rho_{ij}^{(N)}$ is the element of the density matrix, which corresponds to the state with N photons termed intermediate in Section 3, $\chi = \mathbf{Ed}/\hbar$ is the Rabi frequency, Δ is the difference between the laser frequency and the resonance atomic frequency, and T_1 is the energy relaxation time. Although system (33) resembles the Bloch system of equations, it differs from it by the last term in the fourth equation. Since the fourth equation contains the function $\rho_{11}^{(N-1)}$, system of equations (33) for $\rho_{ij}^{(N)}$ is not closed. System (33) at $N = 0$, i.e., for $\rho_{ij}^{(0)}(t) = W_{ij}(t)$, coincides with the previously discussed system (20) and describes the situation whereby intermediate photons are lacking, which corresponds to the first pair of states in Fig. 5, while at $N = 1$ it corresponds to the second pair of states, etc.

It is easy to verify that the four matrix elements

$$\rho_{ij} = \sum_{N=0}^{\infty} \rho_{ij}^{(N)} \tag{34}$$

satisfy the Bloch equations with a phase relaxation constant $1/T_2 = 1/(2T_1)$, i.e., the following equations

$$\begin{aligned}
\dot\rho_{10} &= -\mathrm{i}\left(\Delta - \frac{\mathrm{i}}{2T_1}\right)\rho_{10} + \chi(\rho_{11} - \rho_{00}), \\
\dot\rho_{01} &= \mathrm{i}\left(\Delta + \frac{\mathrm{i}}{2T_1}\right)\rho_{01} + \chi(\rho_{11} - \rho_{00}), \\
\dot\rho_{11} &= -\chi(\rho_{10} + \rho_{01}) - \frac{\rho_{11}}{T_1}, \\
\dot\rho_{00} &= \chi(\rho_{10} + \rho_{01}) + \frac{\rho_{11}}{T_1}.
\end{aligned} \tag{35}$$

A more rigorous derivation of Eqns (33) can be found in the author's paper [49] and monograph [11]. The consideration carried out in Ref. [11] allowed the following conclusion: formulas (27)–(29) are valid in this case, too. All one needs to do in these formulas reduces to replacing the probabilities W_1, W_0, ρ_1, and ρ_0, which were determined from the balance equations, with the probabilities W_{11}, W_{00}, ρ_{11}, and ρ_{00} that should be obtained from Eqns (33) and (35) taking into account the phase relaxation.

In book [11], this problem was also analyzed with the inclusion of electron–phonon interaction which affects the phase relaxation rate. In the simplest variant, the influence of phonons reduces to replacement of the phase relaxation rate $1/(2T_1)$ in Bloch equations (35) with a constant $1/T_2$ which includes the effect of phonons. In this more general case which takes into account the interaction with phonons, the full two-photon correlator is described by the formula

$$p(t) = \frac{\rho_{11}(t)}{T_1}, \tag{36}$$

where $\rho_{11}(t)$ is found from the Bloch equations with a constant T_2 taking into account the effect of phonons.

When counting the photon pairs, the signal has to be accumulated over several milliseconds or longer. For a fixed acquisition interval, the signal magnitude will be proportional to the count rate for the corresponding pairs. The count rate for the photon pairs separated by an interval T in the start–stop mode and for all photon pairs separated in time by T, i.e., the number of the corresponding pairs counted per unit time, is proportional to the corresponding $s(t)$ and $p(t)$ correlators.

Figure 6 depicts the dependences of the start–stop correlator and the full two-photon correlator on the time delay; the dependences were calculated with the aid of equations (20) and Bloch equations (35) subject to the initial condition $W_{00}(0) = 1$ and $\rho_{00}(0) = 1$. The tending of the correlators to zero for short times is termed photon antibunching. Antibunching reveals a simple fact: in linear spectroscopy, a single molecule cannot radiate two photons simultaneously. Antibunching was established in experiment [1, 50].

6. Photon statistics in single-atom fluorescence

Formulas (29) and (31) enable the calculation of the photon distribution function $w_N(T)$, i.e., the function which defied calculation for a single atom employing the Mandel formula (1) [55]. Formulas (31) also permit us to calculate the first and second factorial moments

$$\begin{aligned} \langle N(T)\rangle &= \sum_{N=0}^{\infty} N w_N(T)\,, \\ \langle N^{(2)}(T)\rangle &= \sum_{N=0}^{\infty} N(N-1)\, w_N(T)\,, \end{aligned} \tag{37}$$

and, therefore, the Mandel parameter.

Substituting the probability in the form $W_1(t) = \exp(-kt)$ into expression (29), where k is the rate of stimulated transitions, gives the Poisson distribution for the probability of the number of emitted photons:

$$w_N(T) = \frac{(kT)^N}{N!}\exp(-kT)\,.$$

However, it is evident that the real probability $W_1 = s(t)T_1$, which takes into account photon antibunching, cannot be described obviously by an exponent alone (see Fig. 6). The distribution of photons emitted by this system will therefore follow a non-Poisson distribution. The photon statistics in the system under consideration will, unlike the Poisson one, depend on two parameters: the stimulated transition probability k, and the spontaneous transition probability $1/T_1$. It is precisely the antibunching that determines the sub-Poisson statistics of the photons emitted by a single atom [55], which is confirmed in experiment [56].

7. Photon bunching in fluorescence. A molecule with a triplet level

In Sections 3 – 6, we put forth the theoretical approach to the investigation of the emission of fluorescence photons by a two-level molecule under continuous light excitation. However, almost every organic molecule possesses a triplet level residing between the ground level and the first excited singlet level, which radically changes the fluorescence photon dynamics.

Figure 7 depicts the typical diagram of the lower energy levels for an organic molecule. Such a molecule continuously irradiated by light will execute jumps between the ground and first excited singlet electronic levels, with the absorption and emission of one photon in each event. However, since the intercombination molecular transition probability Γ_{TS} is nonzero, the molecule will occupy sometimes the ground state and reside in it during its lifetime $1/\gamma_{ST}$, which is several milliseconds long. The train of photons with random time intervals between them will therefore alternate with rather long random dark intervals void of radiation — photons will be radiated as if in bunches. This phenomenon has received the name photon bunching.

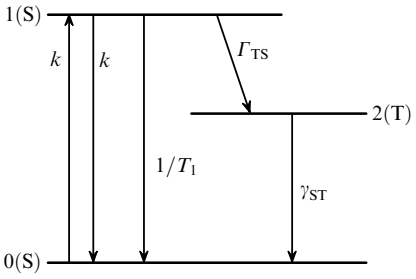

Figure 7. Diagram of the lower energy levels for organic molecules.

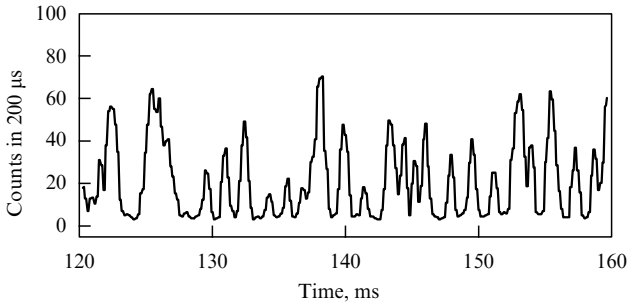

Figure 8. Fluorescence fluctuations of a single 'Red Texas' fluorophore associated with an individual DNA fiber (TR-DNA) at $T = 300$ K [13].

Figure 8 portrays emission of this kind. To the time intervals with fluorescence (the on-intervals) there correspond intervals during which the molecule is in singlet electronic states and executes quantum jumps between the ground and excited electronic states. When the molecule executes a quantum jump to the triplet state, the fluorescence vanishes and an off-interval sets in.

The sequence of random on- and off-intervals characterizes the slow molecular dynamics on the millisecond scale, arising from molecular transitions from the singlet state to the triplet state and reverse ones. The slow molecular kinetics resulting from singlet – triplet transitions may be treated without the inclusion of nondiagonal elements of the density matrix, i.e., on the basis of balance equations for diagonal elements. The equations that correspond to the energy level diagram shown in Fig. 7 are of the form

$$\begin{aligned} \dot\rho_1 &= -(\Gamma + k)\,\rho_1 + k\rho_0\,, \\ \dot\rho_0 &= \left(\frac{1}{T_1} + k\right)\rho_1 - k\rho_0 + \gamma_{ST}\,\rho_2\,, \\ \dot\rho_2 &= \Gamma_{TS}\,\rho_1 - \gamma_{ST}\,\rho_2\,, \end{aligned} \tag{38}$$

where

$$k = 2\chi^2\,\frac{1/T_2}{\Delta^2 + (1/T_2)^2}\,, \qquad \Gamma = \frac{1}{T_1} + \Gamma_{TS}\,. \tag{39}$$

The physical meaning of all constants appearing in these equations becomes clear from Fig. 7, and the constant $1/T_2$ is the optical dephasing rate determined by electron – phonon interaction.

With the aid of system (38), we calculate the two-photon correlator $p(t) = \rho_1(t)/T_1$ to arrive at the formula

$$\begin{aligned} p(t) = \frac{k}{T_1}\Bigg[\frac{\gamma_{ST}}{\gamma_0^2 - R^2} + \left(1 - \frac{\gamma_{ST}}{\gamma_0 - R}\right)\frac{\exp\left[-(\gamma_0 - R)t\right]}{2R} \\ - \left(1 - \frac{\gamma_{ST}}{\gamma_0 + R}\right)\frac{\exp\left[-(\gamma_0 + R)t\right]}{2R}\Bigg]\,, \end{aligned} \tag{40}$$

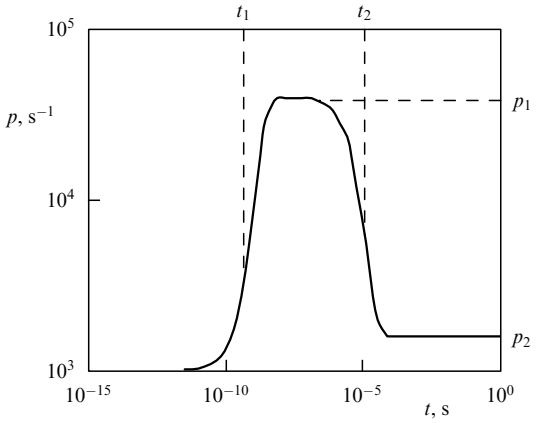

Figure 9. Two-photon correlator of a molecule with a triplet energy level exposed to resonance excitation corresponding to the following values of constants: $T_2 = 5 \times 10^{-11}$ s, $T_1 = 5 \times 10^{-9}$ s, $\chi = 4 \times 10^7$ s^{-1}, $\gamma_{ST} = 2 \times 10^4$ s^{-1}, and $\Gamma_{TS} = 9/T_1$.

where

$$\gamma_0 = \frac{\Gamma + 2k + \gamma_{ST}}{2}\,, \qquad R = \sqrt{\left(\frac{\Gamma + 2k - \gamma_{ST}}{2}\right)^2 - \Gamma_{ST} k}\,. \tag{41}$$

Calculation by formula (40) yields the two-photon correlator depicted in Fig. 9. On the logarithmic time scale, the exponential relaxation appears like a smooth step occupying one order of magnitude on the time scale. The logarithmic scale on the time axis makes it possible to depict on a common drawing the relaxation processes whose relaxation constants differ by several orders of magnitude. The characteristics of this curve, indicated in Fig. 9, have the following physical interpretation: p_1 defines the average photon-pair count rate on the on-interval, p_2 the average on-interval count rate, time t_2 the average value of the sum of on- and off-intervals, and t_1 the average filling time of excited electronic level upon the emission of a photon by the molecule. Available theory [3, 4] also permits the calculation of the on- and off-interval distribution function.

7.1 On- and off-interval distributions

Clearly, the probability ρ_1 that a molecule resides in the excited electronic state is coincident with the probability that the molecule occupies the on-state. The on- and off-interval durations are defined by the duration of stay in the singlet and triplet molecular states, respectively. It is evident that the probability of observing the on- and off-intervals should tend to zero with an increase in their durations. That is why it is impossible to find the on- and off-interval distribution functions employing the system of equations (38), because the obvious conservation law $\rho_1 + \rho_2 + \rho_3 = 1$ follows from Eqns (38). Described in Sections 7.1.1–7.1.3 is a way of deriving the equations for the calculation of the probabilities ρ_{on} and ρ_{off}.

7.1.1 On-state equations. These equations may be developed with the aid of system (38) if we discard in the second equation the term $\gamma_{ST}\,\rho_2$ describing the triplet-to-singlet state molecular transition. Hence, we arrive at the system of equations which describe the on-state dynamics:

$$\begin{aligned} \dot\rho_1 &= -(\Gamma + k)\,\rho_1 + k\rho_0\,, \\ \dot\rho_0 &= \left(\frac{1}{T_1} + k\right)\rho_1 - k\rho_0\,. \end{aligned} \tag{42}$$

The function $w_{on} = \text{const}\,\rho_1$, which was found from these two equations subject to the initial condition $\rho_0(0) = 1$ and was integrally normalized to unity, will describe the distribution of the on-intervals in duration.

System (42) may be further simplified when it is considered that the average time interval separating the jumps between the singlet 1 and 0 states is significantly shorter than the duration of stay in the molecular singlet state. For such frequent jumps between the states 0 and 1, the probability that the molecule occupies the singlet state, viz.

$$\rho_{on} = \rho_1 + \rho_0\,, \tag{43}$$

is exactly the probability of its being in the on-state. For a time far greater than T_1, we may resort to the quasistationary approximation by setting $\dot\rho_1 = 0$. Under this approximation, we arrive with the aid of system (42) at the following equation for the probability of finding the molecule in the on-state:

$$\dot\rho_{on} = -\frac{\rho_{on}}{\tau_{on}}\,, \tag{44}$$

where

$$\frac{1}{\tau_{on}} = k\,\frac{\Gamma_{TS} T_1}{1 + \Gamma_{TS} T_1} = k\,Y_{ISC}\,. \tag{45}$$

Here, Y_{ISC} is the quantum yield of intercombination conversion. The solution of Eqn (44), integrally normalized to unity, is the function

$$w_{on} = \frac{1}{\tau_{on}} \exp\left(-\frac{t}{\tau_{on}}\right) \tag{46}$$

which describes the probability density for discovering an on-interval of duration t. Clearly, τ_{on} is the average on-interval duration, which depends on the pump intensity k in such a way that the average on-interval duration shortens with increasing pump intensity.

7.1.2 Off-state equations. When a molecule occupies a triplet state, its fluorescence terminates. Consequently, one has

$$\rho_{off} = \rho_2\,, \tag{47}$$

which describes the probability that the molecule resides in the off-state. The equation for the probability of finding the molecule in the off-state may be obtained if we discard in the third equation of system (38) the term $\Gamma_{TS}\,\rho_1$ describing the on-to-off state transition of the molecule. The off-state dynamics is therefore governed by the equation

$$\dot\rho_{off} = -\gamma_{ST}\,\rho_{off}\,, \tag{48}$$

whence it follows that the probability density for finding the molecule in the off-state is given by

$$w_{off} = \gamma_{ST} \exp\left(-\gamma_{ST} t\right), \tag{49}$$

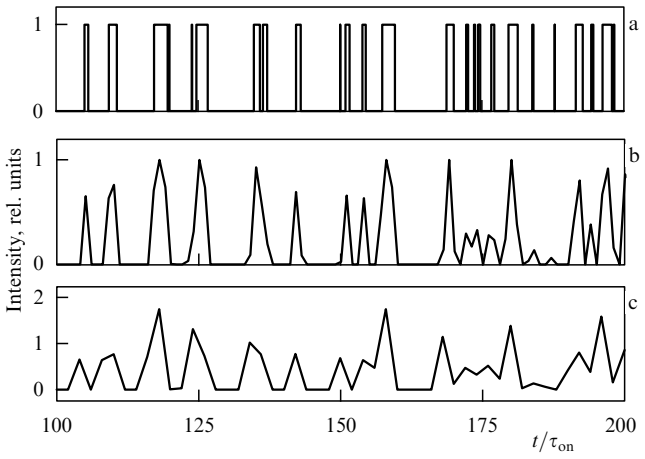

Figure 10. Fluorescence fluctuations calculated employing Eqn (51) for $\tau_{on} = 1$ ms and $\tau_{off} = 3$ ms (a), and fluorescence fluctuation change for an accumulation time $t_{int} = \tau_{on}$ (b) and $t_{int} = 2\tau_{on}$ (c).

where

$$\tau_{off} = \frac{1}{\gamma_{ST}} \tag{50}$$

is the average off-interval duration independent of the pump intensity. We emphasize the following important circumstance. Since Eqns (42) and (48) where obtained from the system of equations (38), which describes the dynamics of the system under consideration, by discarding certain terms, one may gain the impression that Eqns (42) and (48), which were derived to determine the on- and off-interval distributions, are approximate. This fallacy is begotten by the way in which they were derived. As a matter of fact, *Eqns* (42) *and* (48) *are exact for the desired distribution functions of the system involved.*

7.1.3 Equation for fluctuation calculations. The on-to-off state transitions and reverse ones will occur at random points in time with the probabilities described by formulas (46) and (49). To find these random instants, we take advantage of the equation

$$\mathrm{rnd}\,(1) = \int_0^t w(\tau)\,\mathrm{d}\tau\,, \tag{51}$$

where the function rnd (1) determines a random number with a uniform probability density in the range between 0 and 1. The t values determined from Eqn (51) are just the random points in time distributed with a probability density $w(t)$.

Figure 10 illustrates the fluorescence intensity fluctuations calculated in this way. The fluctuations in Fig. 10a represent the fluctuations of molecular residence in the singlet (the ordinate value is equal to unity) and triplet (the ordinate value is equal to zero) states. During its residence in the singlet state, the molecule fluoresces but does not do so in the triplet state, and therefore depicted in Fig. 10a are the fluorescence intensity fluctuations in the ideal case whereby the photon accumulation time is infinitely short. That is why the fluorescence intensity distribution in Fig. 10a is appreciably different from the experimentally found distribution which is plotted in Fig. 8.

In a real experiments there is a signal acquisition time t_{int} during which the fluorescence photons are counted. This signifies that the whole time axis is divided into segments of length t_{int}, and the number of all the photons counted during the interval t_{int} is plotted on the ordinate axis. When the photon accumulation time is comparable to or greater than the average on-interval duration, the picture of fluctuations radically changes and approaches that observed in a real experiment. This is easy to verify by comparing Figs 10b and 8. Measurements of the on- and off-interval distributions in fluorescence intensity fluctuations, depicted in Fig. 10a, show that these functions are really described by the exponential dependences (46) and (49), with the aid of which these fluctuation curves were constructed.

7.2 Fluorescence autocorrelation function

Having at our disposal the record of the fluctuating fluorescence of a single molecule, we can directly measure the probability of fluctuation-generating processes and compare it with the full two-photon correlator. The question concerns the second-order autocorrelation function (AF) determined in experiment and denoted, as a rule, by $g^{(2)}(t)$ [1, 41]. The autocorrelation function is commonly defined as

$$g^{(2)}(\tau) = \lim_{t\to\infty} \frac{\langle I(t)\, I(t+\tau)\rangle}{\langle I(t)\rangle^2}\,, \tag{52}$$

where $I(t)$ is the fluctuating fluorescence intensity similar to that represented in Figs 8 and 10. The autocorrelation function tends to unity for an infinite delay τ. In practice, the determination of AF reduces to multiplication of the measured fluctuating fluorescence intensity, like the function plotted in Fig. 8, by itself shifted by a time τ.

The overlap integral taken of two quantum trajectories shifted by τ and normalized to unity for $\tau \to 0$ will be referred to as the autocorrelator C:

$$C(\tau) = \frac{\langle I(t)\, I(t+\tau)\rangle}{\langle I^2(t)\rangle} = \frac{\int_{-\infty}^{\infty} I(t)\, I(t+\tau)\,\mathrm{d}t}{\int_{-\infty}^{\infty} I^2(t)\,\mathrm{d}t}\,. \tag{53}$$

There is a simple relation between the experimentally obtained AF $g^{(2)}(\tau)$ and the autocorrelator $C(\tau)$, on the one hand, and the theoretically evaluated two-photon correlator $p(\tau)$, on the other hand [45, 57]:

$$C(\tau) = \frac{p(\tau)}{k}\,, \qquad g^{(2)}(\tau) = \frac{p(\tau)}{p(\infty)}\,. \tag{54}$$

When the magnitudes of the constants $1/T_1$ and k, which define the time t_1 (see Fig. 9), are far greater than the magnitudes of the constants Γ_{TS} and γ_{ST}, which define the slow dynamics, i.e., the time t_2 in that same Fig. 9, the two-photon correlator defined by formula (40) for $\tau \gg T_1$ may be expressed in terms of the average on- and off-interval durations:

$$p(\tau) = \frac{k}{1/\tau_{on} + 1/\tau_{off}} \left\{ \frac{1}{\tau_{off}} + \frac{1}{\tau_{on}} \exp\left[-\left(\frac{1}{\tau_{off}} + \frac{1}{\tau_{on}} \right)\tau \right] \right\}, \tag{55}$$

where the average on- and off-interval durations are defined by formulas (45) and (50). An expression similar to formula (55) was also obtained by Verberk and Orrit [58].

If we construct the correlator $C(\tau)$, i.e., the left side of the first of Eqns (54), with the aid of the fluctuating intensity function plotted in Fig. 10a and calculate the ratio $p(\tau)/k$ by

formula (55), i.e., construct the function on the right-hand side of the first of formulas (54), they will coincide with each other. We are reminded that the probability densities $w(t)$ and simple equations (44) and (48) for determining the on- and off-interval probabilities were obtained from exact system (38) by discarding certain terms, i.e., as if by moving to 'approximate' equations. However, the autocorrelation function found with the aid of random quantum intensity trajectories (QITs) calculated by these 'approximate' equations is nevertheless practically coincident with the two-photon correlator $p(\tau)$ obtained by way of solution of exact system (38). This coincidence paves the way for two nontrivial implications:

(1) The method of obtaining the equations describing the on- and off-interval distributions, which was proposed in Refs [3, 4, 11] and described in Section 7.1, is correct.

(2) There is a simple relation between the *experimentally* obtained correlator $C(\tau)$, which appears on the left-hand side of the first of formulas (54), and the *theoretically* evaluated photon-pair count rate $p(\tau)$, which appears on the right sides of formulas (54) — measuring the correlator $C(\tau)$ or the AF is equivalent to counting the photon pairs in SMS.

It should be emphasized that with the aid of QITs we can obtain both the on-/off-interval distribution functions and the two-photon correlator. By employing only the measured two-photon correlator it is possible to find the left sides of the following equations

$$\frac{1}{\tau_0}=\frac{1}{\tau_{\rm on}}+\frac{1}{\tau_{\rm off}}\,,\qquad \frac{p(0)}{p(\infty)}=\frac{\tau_{\rm on}}{\tau_{\rm on}+\tau_{\rm off}}\,, \tag{56}$$

and from this determine the average on-/off-interval durations. However, there is no way of calculating the on-/off-interval distribution functions with the aid of the two-photon correlator.

8. A molecule in a fluctuating environment

As noted in Section 2, even the first experiments with single molecules introduced into polymer matrices exhibited spectral line jumps occurring on a scale ranging from several milliseconds to several dozen seconds. Suchlike jumps are exemplified in Fig. 11a. These jumps signify that the absorption coefficient of a single molecule fluctuates. Indeed, an optical line with one resonance frequency is measured in one laser scanning, and a line with another frequency in another laser scanning. At the same time, it was recognized that these absorption coefficient fluctuations are due to the existence of interaction between the chromophore of the molecule and the TLSs of polymers and glasses.

According to Anderson's model [37], TLSs may be described in the context of a model that uses a two-well adiabatic potential in some configuration coordinate, which is plotted in Fig. 11b showing all transitions — both vertical optical transitions in the molecule and horizontal tunnel transitions in the TLS, which define the dynamics of this system. Levels 0 and 2 belong to the electronically nonexcited impurity molecule, and levels 1 and 3 to the electronically excited one.

8.1 Theory of the time-dependent absorption coefficient

One can see from Fig. 11a that the absorption spectrum of a single molecule depends on the duration of laser scanning. This brings up the question of the method for calculating the

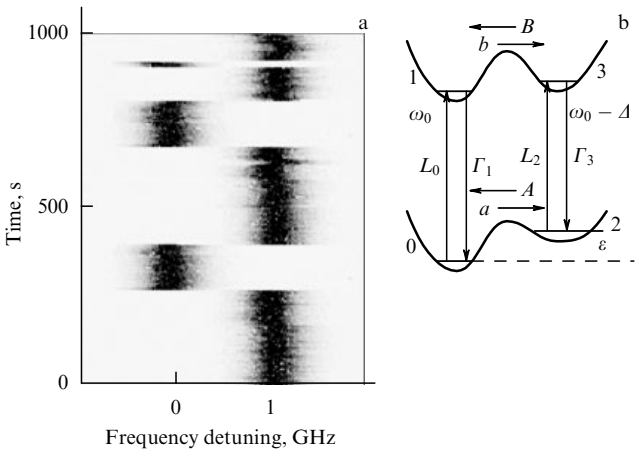

Figure 11. (a) Jumps of the spectral line of a single tetra-*tert*-butyl terrylene molecule introduced into polyisobutylene at $T = 7$ K [40]. The laser scan duration is 8 s. (b) Energy level diagram describing a molecule which strongly interacts with one TLS.

absorption coefficient of a single molecule that would contain the measuring time. Two lines of attack on the problem have been advanced.

The first line, which was suggested by the author of this review, involves extending the dynamic theory for an optical band, which the author had earlier formulated [59, 60] for a chromophore interacting with equilibrium TLSs, to the case of nonequilibrium TLSs. This generalization was made in Ref. [61], where the equilibrium density matrix for the TLS was replaced with a nonequilibrium one, i.e., dependent on the initial conditions. This is a purely dynamic approach to the problem of the fluctuating absorption coefficient. More recently, the replacement of the equilibrium density matrix for a TLS with a nonequilibrium one was substantiated in Refs [62, 63], resulting in the development of a consistent dynamic theory of the fluctuating absorption coefficient. For the first time, this theory was applied to experimental data processing in Refs [57, 64]. Zheng and Brown [53, 54] and Kilin et al. [65] also employed the dynamic approach in SMS, although for the solution of some other problems.

The second line combines the dynamic and stochastic approaches and was employed in Refs [46, 47, 66–76]. The dynamic and stochastic approaches were combined in different ways. For instance, the Schrödinger equation included the assumption of fluctuating energy [66, 70], and the fluctuating resonance frequency was artificially introduced into the optical Bloch equations [46, 47].

Since the purely dynamic approach is the most consistent one, there is good reason to consider the problem of the fluctuating absorption coefficient by invoking precisely this approach. Such an approach, which involves using the system's Hamiltonian and the equations for the density matrix, obtained on the basis of this Hamiltonian, necessarily brings into existence the initial conditions for the TLS in the expression for the absorption coefficient.

Indeed, the evolution of a quantum system is defined by the equation

$$\Psi(t+t_0)=\exp\left(-\frac{{\rm i}H}{\hbar}\,t\right)\Psi(t_0)=\exp\left[-\frac{{\rm i}H}{\hbar}(t+t_0)\right]\Psi(0)\,, \tag{57}$$

where H is the total Hamiltonian of the system, and $\Psi(t_0)$, $\Psi(0)$ are the different initial states of the system. According to Eqn (57), the state of the system at any instant of time may be treated as the initial one. The formulas of the dynamic theory for the absorption coefficient should also include the initial conditions. How can this be achieved?

The diagram shown in Fig. 11b describes the chromophore – TLS interaction. When the TLS is in thermal equilibrium with the medium, the absorption coefficient of this system may be represented as

$$k(t,\omega) = \big(1 - f(T)\big)\, L_0(\omega) + f(T)\, L_2(\omega)\,, \tag{58}$$

where the Lorentzians

$$\begin{aligned} L_0(\omega) &= 2\chi^2\, \frac{1/T_2}{(\omega-\omega_0)^2 + 1/T_2^2}\,, \\ L_2(\omega) &= 2\chi^2\, \frac{1/T_2}{(\omega-\omega_0+\Delta)^2 + 1/T_2^2} \end{aligned} \tag{59}$$

describe the absorption lines corresponding to the $0-1$ and $2-3$ interstate transitions, and T_2 is the optical dephasing time which accounts for rapid jumps in the picosecond range. The coefficients of the Lorentzians in expression (58), which contain the function $f(T) = \big(\exp(\varepsilon/k_{\rm B}T) + 1\big)^{-1}$, where ε according to Fig. 11b is the level splitting in the TLS, and $k_{\rm B}$ is the Boltzmann constant, are the probabilities that the system occupies the initial state for light absorption under thermal equilibrium at a temperature T.

Under continuous excitation by light, the system, upon the emission of a photon corresponding to the $0-1$ transition, finds itself in the state 0 with a probability equal to unity. This is a nonequilibrium probability, and it will therefore begin to change with time. To take this into account, we should replace the equilibrium probability with the nonequilibrium one, i.e., bring about the following change in expression (58):

$$f(T) \to \rho(t,T) = f(T) + \big(\rho(0) - f(T)\big)\, \exp(-Rt)\,, \tag{60}$$

where $R = a + A$. The physical meaning of the relaxation constants a and A is elucidated by Fig. 11b. The time and initial conditions will appear in formula (58) after this change. For instance, if the instant of photon emission via the $0-1$ transition is taken to be zero, we must put $\rho(0) = 0$ in formula (60). It is easily verified that the probability (60) is also amenable to time translation, as in formula (57), namely

$$\begin{aligned} \rho(t+t_0,T) &= \rho(\infty) + \big(\rho(t_0) - \rho(\infty)\big)\, \exp(-Rt) \\ &= \rho(\infty) + \big(\rho(0) - \rho(\infty)\big)\, \exp\big[-R(t+t_0)\big]\,. \end{aligned} \tag{61}$$

It is precisely the inclusion of initial conditions that enables the dynamic theory to adequately describe the quantum jumps of a spectral line, because every quantum jump signifies a change in the initial conditions. This will be shown clearly in Section 8.3.

A disadvantage of the above way of introducing nonequilibrium features into the formula for the absorption coefficient, which was first employed in Ref. [61], is the lack of a rigorous mathematical substantiation of the validity of the change made. More recently, the possibility of such a change was rigorously substantiated in Refs [62, 63]. It was established that this change can really be effected if one takes into account the smallness of the parameter $T_1 R$, where T_1 is the energy relaxation time, and R is the tunnel relaxation rate.

A more rigorous theory [11] yields the following expression for the time-dependent absorption coefficient depending also on the initial conditions:

$$k(\omega,t) \propto d^2 \int_{-\infty}^{\infty} I_{\rm TLS}(y,t) \exp\left[-{\rm i}\left(\omega - \frac{\rm i}{T_2(t)}\right) y\right] {\rm d}y\,, \tag{62}$$

where the function

$$\begin{aligned} \exp\left(-\frac{y}{T_2(t)}\right) I_{\rm TLS}(y,t) &= \exp(-{\rm i}\omega_0 y) \exp\left(-\frac{y}{T_2(t)}\right) \\ &\times \prod_{j=1}^{N} \left[1 - \frac{\Delta_j}{\Delta_j - {\rm i}R_j}\, \rho_j(t) \big(1 - \exp\big(-{\rm i}(\Delta_j - {\rm i}R_j)\, y\big)\right] \end{aligned} \tag{63}$$

describes the time dependence of the dipole correlator of the system consisting of the chromophore and the TLS set interacting with it. Here, Δ_j is the change in TLS splitting under electronic excitation of the molecule, and R_j is the TLS relaxation rate. The function

$$\rho_j(t) = \rho_j(\infty) - \big(\rho_j(0) - \rho_j(\infty)\big)\, \exp(-R_j t) \tag{64}$$

describes the relaxation of a TLS removed from the equilibrium state by a quantum jump at the zero point in time, and

$$\rho_j(\infty) = f_j(T) = \left(1 + \exp\frac{\varepsilon_j}{kT}\right)^{-1}, \tag{65}$$

where ε_j is the TLS level splitting, describes the equilibrium probability that the TLS is found in the upper level. The integration with respect to y in expression (62) is actually performed over an interval having a duration of several T_2 and comprising the time t.

The dynamic theory permits the establishment of a simple relation between the absorption coefficient of a single molecule, which is commonly measured by laser frequency scanning, and the two-photon correlator, i.e., the AF. Osad'ko and Yershova [57, 64] have made good use of this theory to process the experimentally obtained autocorrelation functions $g^{(2)}(\tau)$.

An entirely different approach to the calculation of the time-dependent absorption coefficient was taken by Geva and Skinner [67, 68], which was also employed by other authors [46, 47]. In Refs [67, 68], the problem of scanning-time introduction into the formula for the absorption coefficient was solved on the assumption that only the TLSs that have reached thermal equilibrium, i.e., the TLSs whose populations from this point on depend only on the temperature, are capable of making a contribution to the dipole correlator. This assumption is reflected in the model adopted in these papers for the dipole correlator of a single molecule interacting with one TLS of the polymer:

$$I_j = \begin{cases} I_j(t,T,R_j)\,, & R_j > \dfrac{1}{t}\,, \\ 1\,, & R_j < \dfrac{1}{t}\,, \end{cases} \tag{66}$$

where R_j is the relaxation rate of the jth TLS. In the approach pursued by Geva and Skinner, the scanning time determines how many cofactors for a given scanning time should be left in

the product

$$I(t, t_{sc}) = \prod_{j=1}^{N(t_{sc})} I_j \tag{67}$$

which describes the dipole correlator of the molecule interacting with all TLSs of the polymer. The jth-TLS contribution described by the function $I_j(t, T, R_j)$ is independent of the scanning duration. The unity on the right-hand side of formula (66) signifies that the contribution from nonequilibrium TLSs to the optical band of a single molecule is ignored. This drawback of the Geva – Skinner theory was discussed by Plakhotnik [69]; in an attempt to take into account the fluctuating absorption coefficient, he considered a quantity which is, in our notation, expressed as

$$S(\omega', \tau) \propto \int_0^{\omega_0} k(\omega, 0)\, k(\omega + \omega', \tau)\, \mathrm{d}\omega\,, \tag{68}$$

where k is the absorption coefficient measured by way of laser scans. However, this formula, being differed from the formula for the two-photon correlator only in that every Lorentzian in it is replaced with a convolution of two Lorentzians, does not solve the problem of calculating the fluctuating absorption coefficient.

Following the Geva – Skinner approach, Barkai et al. [77] considered cumulants of different types in connection with the problem of calculation of the moments of optical bands. The moments of optical band distributions for single molecules were measured by Naumov et al. [78].

8.2 Role of near and far two-level systems in optical band formation

In the above-cited papers [67, 68], Geva and Skinner calculated the optical band shape with the inclusion of the effect of several hundred TLSs and the employment of computer simulations of TLS parameters through the use of random functions. Had they employed a more correct correlator (63) in lieu of correlator (67), the problem of optical band calculation for a single impurity center interacting with a set of TLSs would have been amply solved. Geva and Skinner drew a correct conclusion that not all of the polymer TLSs by far make a significant contribution to the product with respect to j in formula (67), which also follows from formula (63). Indeed, the dipole – dipole chromophore – TLS interaction energy $\Delta(r) = DdF(\vartheta, \varphi)/r^3$, where D and d are the respective dipole moments of the chromophore and the TLS, decreases rapidly with the chromophore – TLS intermolecular distance r. Since Δ is the spacing between the lines, and $2/T_2$ is the half-width of these lines, the condition of resolution of the two lines, viz.

$$\frac{2}{T_2} = \Delta(r) = \frac{Dd}{r^3}\,, \tag{69}$$

may be considered as the equation for the determination of the radius of the closest neighborhood harboring the TLSs which interact most strongly with the chromophore and are therefore capable of giving rise to well-resolved optical lines. It is evident that remote TLSs, for which $\Delta \ll 2/T_2$, can hardly make a contribution to the product (63). Indeed, for terms with such small Δ we have

$$(\Delta - \mathrm{i}R)y \leqslant (\Delta - \mathrm{i}R)T_2 \to 0\,,$$

and therefore the corresponding exponential term in formula (63) turns to unity irrespective of the magnitude of the ratio Δ/R. In other words, the contribution from remote TLSs to the product with respect to j may be neglected. The greatest contribution to the product with respect to j is therefore made by several TLSs residing in the immediate vicinity of the chromophore and obeying the inequality $\Delta > 2/T_2$, which signifies that the separation between the lines exceeds their half-widths. Putting $2/T_2 = 200$ MHz and $D = d = 0.4$ D [79], we find that the radius of the closest neighborhood reaches 1.07 nm, and the volume is 5 nm^3. For a TLS concentration on the order of 5×10^{-21} cm^{-3}, we find that the closest neighborhood of the chromophore contains one to two TLSs. The experiment of Orrit's group [39] testifies that the optical band consists of two lines for 40% of the molecules investigated. This is consistent with our estimate. That is why the situation where the closest neighborhood of the chromophore contains only one TLS holds the greatest practical interest.

8.3 Several absorption coefficients for a single molecule

When the measuring time is shorter than the TLS relaxation time, one molecule may exhibit several absorption coefficients. This is a new effect. We consider this phenomenon through the example of a situation whereby there is only one TLS in the immediate vicinity of the impurity molecule. Then, the impurity center possesses two optical lines arising from the $0-1$ and $2-3$ transitions between the quantum states shown in Fig. 11b. Levels 0 and 2 correspond to the ground electronic state of the impurity molecule for two possible positions of the matrix atom, while levels 1 and 3 to the excited electronic state of the impurity molecule for the same two positions of the matrix atom. When the photon absorption probabilities L_0 and L_2 are comparable to the excited-electronic-state decay probabilities Γ_1 and Γ_3, account should be taken of the $1-3$ transitions along with the $0-2$ transitions. In this case, the frequency of jumps between the left and right well pairs will depend on the exciting laser intensity. Such a model was considered by Kilin et al. [65], who studied the fluorescence of single terrylene molecules in polyethylene versus irradiation power.

For a low exciting radiation intensity, the photon absorption probabilities L_0, L_2 are much lower than the decay probabilities Γ_1, Γ_3 for the excited electronic states. In this case, the transitions between the levels 1 and 3 may be neglected, which signifies neglecting the jumps of the matrix atom, when the impurity is excited. Then, only the probabilities A and a for the transition between the two possible ground states of the impurity molecule are taken into account in the diagram shown in Fig. 11b. At low temperatures, the reciprocal of these probabilities may lie in the time interval from several microseconds to several seconds or even dozens and hundreds of seconds. When observing the jumps on such a temporal scale, the rapid jumps corresponding to the nano- and picosecond ranges are taken into account by the optical dephasing rate $1/T_2$.

We analyze here the effect of only one TLS strongly coupled to the impurity center in the case when the magnitude of spectral line jump is far greater than the linewidth. With the aid of correlator (63) for $\Delta \gg R$, we find the absorption coefficient corresponding to the doublet of lines whose amplitudes are time-dependent:

$$k(t, \omega) = \big(1 - \rho(t, T)\big)\, L_0(\omega) + \rho(t, T)\, L_2(\omega)\,, \tag{70}$$

where the Lorentzians are defined by formulas (59), and a function $\rho(t, T)$ was set out in formula (60). For convenience, the lower-frequency line corresponding to L_2 will be referred to as the red line, and the higher-frequency line corresponding to L_0 as the blue line. The absorption coefficient depends not only on the time, but on the initial conditions as well. The dependence on the initial conditions has the effect that there appear two types of absorption coefficients for the impurity molecule interacting with the TLS. We consider this question in greater detail.

Let the molecule 'jump' into state 2 at some random point in time. At this instant of time, taken as the initial one, $\rho(0) = 1$. We substitute this initial value into expression (60) to arrive at the following expression for the absorption coefficient:

$$k_{\mathrm{r}}(t,\omega) = \frac{A}{R}\left[1 - \exp\left(-Rt\right)\right] L_0(\omega) + \left[\frac{a}{R} + \frac{A}{R}\exp\left(-Rt\right)\right] L_2(\omega)\,. \tag{71}$$

According to formula (71), the detection probability for the red line will decrease with time and the probability for the blue line will increase.

When the molecule 'jumps' to the state 0, $\rho(0) = 0$. We substitute this value into expression (60) to obtain the absorption coefficient which is different from expression (71):

$$k_{\mathrm{b}}(t,\omega) = \left[\frac{A}{R} + \frac{a}{R}\exp\left(-Rt\right)\right] L_0(\omega) + \frac{a}{R}\left[1 - \exp\left(-Rt\right)\right] L_2(\omega)\,. \tag{72}$$

The probability of detecting the blue line will become lower with time, and the probability of observing the red line will rise. For $Rt \gg 1$, formulas (71) and (72) assume the form

$$k = (1-f)L_0 + fL_2\,. \tag{73}$$

For long measuring times, the dependence on the initial conditions therefore vanishes. In this case, the absorption coefficient is time-independent, and the line amplitude ratio in the doublet is only determined by the temperature.

Clearly, the existence of two different absorption coefficients for one molecule is due to the fact that we considered a single molecule that interacts appreciably with only one TLS. Along similar lines it may be shown that a molecule that strongly interacts with two, three, or more TLSs will possess four, eight, etc. absorption coefficients. In Section 9, we will discuss how these absorption coefficients can be measured in experiment.

9. Averaging the fluctuating absorption coefficient

It was shown in Section 8 that the theory predicts the existence of several types of absorption coefficients for short times, i.e., for $Rt \ll 1$. It is precisely for these short measuring times that a fluctuating absorption coefficient is dealt with in experiments. The above-derived formulas (71) and (72) allow description of the experimental data with the fluctuating absorption coefficient. However, the values calculated by formulas (71) and (72) may be compared only with the absorption coefficients averaged in a certain way. In this connection, it is first required to find the averaging procedure whereby the averaged absorption coefficient would be time-dependent.

9.1 Calculation of the fluctuating absorption coefficient

At first we consider how it is possible to calculate the instants of time of random jumps from state 2 to state 0 and back, i.e., how it is possible to simulate the experimentally obtained fluctuations. Clearly, the quantities $1/A = \tau_2$ and $1/a = \tau_0$ determine the system lifetimes in the states corresponding to the left and right pairs of the potential wells in Fig. 11b. Consequently, should the system find itself in state 2 with a unit probability, then

$$W_2(t) = \exp\left(-At\right) \tag{74}$$

describes the probability of discovering the system in state 2 by the point in time t, i.e., the probability that a jump has not occurred. The probability that the system changes to state 0 by the point in time t is described as

$$P_2(t) = 1 - W_2(t) = 1 - \exp\left(-At\right). \tag{75}$$

Since the instant t of jump is random, $P_2(t) = \mathrm{rnd}\,(t)$ represents a random function of time, which assumes values ranging from zero to unity. The random points in time t_2 at which there occurs a jump from state 2 to state 0 may be defined by the formula

$$t_2 = -\frac{1}{A}\ln\left(1 - P_2(t)\right) \tag{76}$$

obtained from Eqn (75). Using this line of reasoning, we find the following expression for the random points in time at which there occurs a transition from state 0 to state 2:

$$t_0 = -\frac{1}{a}\ln\left(1 - P_0(t)\right), \tag{77}$$

where $P_0(t) = \mathrm{rnd}\,(t)$. In the calculation of random instants of jumps, Jung et al. [47] and Kilin et al. [65] also employed equations similar to Eqns (76) and (77). Setting $A = 3a$ for definiteness, we can model the temporal dependence of the system's residence in states 2 and 0 with the aid of formulas (76), (77) and the random function $\mathrm{rnd}\,(t)$.

It would appear reasonable that the fluorescence photon accumulation time t_{int} is proportional to the duration of laser scanning. That is why for short laser scans we will measure only one line in each laser scanning — either red, or blue. With increasing scanning duration, the laser scans in rare instances will culminate in measuring two lines. Lastly, for scans far longer than $1/R$ we will measure the line doublet virtually in every scan. Figure 12 demonstrates the fluctuating optical spectra calculated in Ref. [80] for different values of the signal acquisition interval t_{int}. As noted above, t_{int} is proportional to the laser scan duration.

For short t_{int}, as is seen from the extreme left column of the images in Fig. 12, the optical line jumps randomly between two spectral positions. For medium t_{int}, as evidenced by two middle columns, the spectral line doublet with fluctuating intensities of the doublet components is measured in many laser scans. Lastly, for long t_{int}, which corresponds to the right-most column, the line doublet is measured virtually in every laser scan. This brings up the natural question: how should this fluctuating absorption coefficient be processed with the aid of theoretical formulas

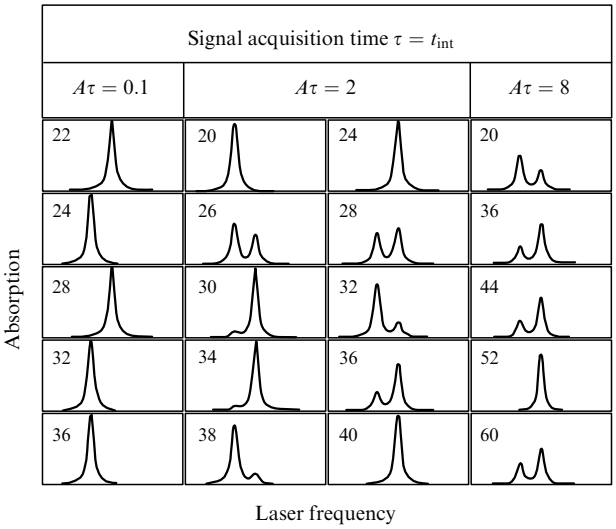

Figure 12. Fluctuations of the absorption coefficient for short laser scans (left column), for medium-long scans (two middle columns), and for long scans (right column). The numbers indicate the dimensionless time in units of At.

(71) and (72)? The averaging procedure is discussed below in Section 9.2.

9.2 Averaged absorption coefficient

The fluctuating absorption coefficient may be averaged in different ways. In this section we outline the averaging procedure leading to two average absorption coefficients which may be directly compared with theoretical expressions (71) and (72). For convenience of discussion, the fluorescence excited with absorption line frequencies corresponding to the $0-1$ and $2-3$ transitions will be termed the 'blue' and 'red' fluorescence, respectively. For 'short' scans, whose duration is far shorter than τ_0 and τ_2, the blue $I_1(t)$ and red $I_3(t)$ fluorescence intensities are directly proportional to the probabilities of the system residence in states 0 and 2, respectively. These functions — quantum intensity trajectories — describe the temporal behavior of the fluorescence under excitation at the ω_0 and $\omega_0 - \Delta$ frequencies, respectively. With their aid it is possible to construct two AFs which may be determined in experiment:

$$g_1^{(2)}(\tau) = \lim_{t\to\infty} \frac{\langle I_1(t+\tau)\, I_1(t)\rangle}{\langle I_1(t)\rangle^2}\,,$$
$$g_3^{(2)}(\tau) = \lim_{t\to\infty} \frac{\langle I_3(t+\tau)\, I_3(t)\rangle}{\langle I_3(t)\rangle^2}\,. \tag{78}$$

The autocorrelation functions are normalized to unity at infinity. However, for convenience of comparison with theoretical expressions it is more expedient to measure the correlator $C(\tau)$ which is related in a simple way to the calculated two-photon correlator $p(\tau)$.

First of all, it should be emphasized that with the use of two QITs we can construct two autocorrelators

$$C_{bb}(\tau) = \frac{\int_{-\infty}^{\infty} I_1(t)\, I_1(t+\tau)\,\mathrm{d}t}{\int_{-\infty}^{\infty} I_1^2(t)\,\mathrm{d}t}\,,$$
$$C_{rr}(\tau) = \frac{\int_{-\infty}^{\infty} I_3(t)\, I_3(t+\tau)\,\mathrm{d}t}{\int_{-\infty}^{\infty} I_3^2(t)\,\mathrm{d}t}\,, \tag{79}$$

and two so-called cross-correlators

$$C_{br}(\tau) = \frac{\int_{-\infty}^{\infty} I_1(t)\, I_3(t+\tau)\,\mathrm{d}t}{\int_{-\infty}^{\infty} I_1^2(t)\,\mathrm{d}t}\,,$$
$$C_{rb}(\tau) = \frac{\int_{-\infty}^{\infty} I_3(t)\, I_1(t+\tau)\,\mathrm{d}t}{\int_{-\infty}^{\infty} I_3^2(t)\,\mathrm{d}t}\,. \tag{80}$$

The fluorescence photons emitted upon system excitation by radiation with the frequencies of the red and blue lines will be referred to as r and b type photons, respectively. During the time interval, when the laser frequency coincides with the frequency of the red line, it is evident that the system emits r-photons, and the b-photons are emitted when it coincides with the frequency of the blue line. There therefore exist nonzero probabilities to detect four photon-pair types: bb, rr, br, and rb. These probabilities are defined by the formulas

$$\mathrm{d}W_{bb}(\tau) = p_{bb}(\tau)\,\mathrm{d}\tau\,, \qquad \mathrm{d}W_{rr}(\tau) = p_{rr}(\tau)\,\mathrm{d}\tau\,,$$
$$\mathrm{d}W_{br}(\tau) = p_{br}(\tau)\,\mathrm{d}\tau\,, \qquad \mathrm{d}W_{rb}(\tau) = p_{rb}(\tau)\,\mathrm{d}\tau\,. \tag{81}$$

The two-photon correlator of a molecule interacting with a set of TLSs of polymers was calculated in Refs [62, 63]. We apply formula (39) from Ref. [63] in the case of a chromophore interacting with one TLS to arrive at

$$p(\tau) = k(\tau, T)\left(1 - \exp\left(-\frac{\tau}{T_1}\right)\right), \tag{82}$$

where k is determined from expressions (71) and (72) at $t = \tau$, and T_1 is the lifetime of the excited electronic level. When the first photon is of the r type, use should be made of formula (71), and formula (72) for a b-type photon. In view of the initial conditions described above, for $\tau \gg T_1$ it is possible to derive the expressions for the four two-photon correlators

$$p_{bb}(\tau) = \left(\frac{A}{R} + \frac{a}{R}\exp(-R\tau)\right) L_0(\omega)\,,$$
$$p_{br}(\tau) = \frac{a}{R}\left(1 - \exp(-R\tau)\right) L_2(\omega)\,,$$
$$p_{rb}(\tau) = \frac{A}{R}\left(1 - \exp(-R\tau)\right) L_0(\omega)\,,$$
$$p_{rr}(\tau) = \left(\frac{a}{R} + \frac{A}{R}\exp(-R\tau)\right) L_2(\omega)\,. \tag{83}$$

We note that the expressions for the p_{bb} and p_{rr} autocorrelators coincide with those derived by Kilin et al. [65] if it is assumed that the exciting laser intensity is low (cross-correlators were not considered in Ref. [65]). It is easily seen that the two-photon correlators are closely related to the two absorption coefficients defined by formulas (71) and (72). We will dwell on this question in greater detail.

The symbols in Fig. 13a display the auto- and cross-correlator magnitudes calculated by formulas (79) and (80) by way of computer QIT simulation. Naturally, the above correlators can also be determined in experiment. The curves at the left of Fig. 13 portray the Lorentzian amplitudes calculated by formulas (71) and (72). A comparison of the correlators obtained from numerical experiments (symbols) with the two-photon correlators calculated by quantum-mechanical techniques (curves) showed that the following

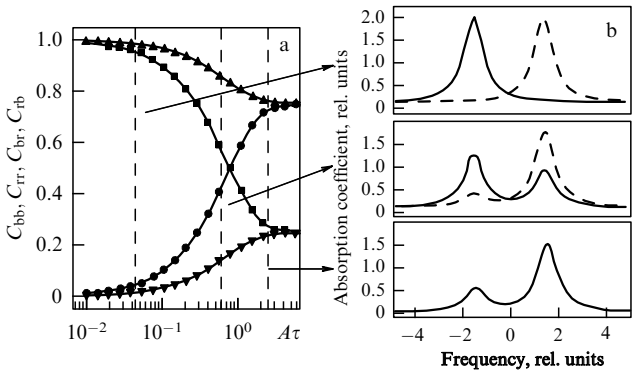

Figure 13. (a) Auto- and cross-correlators: ■ — C_{rr}, ▲ — C_{bb}, ● — C_{rb}, and ▼ — C_{br} calculated employing two QITs; solid lines — calculated amplitudes of the Lorentzians in formulas (83). (b) Absorption coefficients calculated by formulas (85) for the time delays whereto the vertical dashed lines in figure a correspond.

simple relationships exist:

$$C_{bb}(\tau)=\frac{p_{bb}(\tau)}{L_0}\,,\qquad C_{rr}(\tau)=\frac{p_{rr}(\tau)}{L_2}\,,$$
$$C_{br}(\tau)=\frac{p_{br}(\tau)}{L_2}\,,\qquad C_{rb}(\tau)=\frac{p_{rb}(\tau)}{L_0}\,. \tag{84}$$

The four two-photon correlators are functions of exciting radiation frequency, and functions of time delay for emitted photon pairs. If we construct, with the aid of auto- and cross-correlators found in experiment with the use of QITs, the following frequency functions

$$k_r(\tau,\omega)=C_{rb}(\tau)\,L_0(\omega)+C_{rr}(\tau)\,L_2(\omega)\,,$$
$$k_b(\tau,\omega)=C_{bb}(\tau)\,L_0(\omega)+C_{br}(\tau)\,L_2(\omega)\,, \tag{85}$$

they will coincide with the absorption coefficients k_r and k_b calculated by formulas (71) and (72). Formulas (85) furnish the expressions for two averaged absorption coefficients which may be compared with the two absorption coefficients worked out theoretically by formulas (71) and (72). Consequently, formulas (85) indicate how to process QITs and pass from the fluctuating absorption coefficient to two averaged coefficients in such a way that these averaged absorption coefficients could be compared with the absorption coefficients evaluated by theoretical formulas.

Figure 13b shows the absorption coefficients k_r and k_b calculated by formulas (85) for the time delays indicated by the vertical lines in Fig. 13a. For a time delay satisfying the condition $R\tau \ll 1$, we arrive at two averaged absorption coefficients, each of which corresponds to one spectral line. For a longer time delay satisfying the condition $R\tau \sim 1$, each averaged absorption coefficient corresponds to a line doublet. Lastly, for a very long delay satisfying the condition $R\tau \gg 1$, we arrive at the single absorption coefficient corresponding to the line doublet.

10. Temporal broadening of the optical band of a single molecule

In Section 9.2, we considered a method of determining the averaged absorption coefficients which may be compared with the theoretically predicted absorption coefficients. This method is only adequate when the lines of the optical band are clearly separated from each other on the frequency scale. However, the case when the lines of one optical band appreciably overlap is quite often encountered in experiment, and the method described in Section 9.2 is inapplicable. Then, to compare experimental and theoretical findings, advantage can be taken of the method involving measurements of the half-width of the complex optical band and its comparison with the theoretically determined half-width. In this connection, the problem of optical line broadening will be our initial concern.

The temperature broadening of the phononless lines emitted by impurity centers in crystals, polymers, and glass has been the subject of numerous experimental and theoretical works (see reviews [81, 82] and references cited therein). The electron – phonon interaction is responsible for this broadening in crystals, while in polymers and glass it is added with the interaction with TLS excitations. The latter defines the low-temperature behavior of the PLL half-widths for impurity centers in polymers and glass [82 – 84].

It is pertinent to note that the chromophore – TLS interaction problem is mathematically equivalent to the problem of the interaction of a spin resonant to microwave radiation with the ensemble of other nonresonance spins. Fifty years ago this problem was solved by Anderson [85] in the framework of the stochastic approach and, as shown in Ref. [11], yields an expression for the dipole correlator, which coincides with formula (63) if the nonequilibrium TLS population $\rho(t)$ is replaced in it with the equilibrium one, $\rho(\infty)=f(T)$. Then, the following formula results for the absorption coefficient in the case of interaction with only one TLS, i.e., for the model depicted in Fig. 11b, and disregarding the tunneling in the excited electronic state — that is, for $b=B=0$:

$$k(\omega)=2\chi^2\begin{cases}(1-f)\dfrac{\gamma_0}{(\omega-\omega_0)^2+\gamma_0^2}+ & \\ \quad+f\,\dfrac{\gamma_0+\gamma}{(\omega-\omega_0-\Delta)^2+(\gamma_0+\gamma)^2}\,, & \Delta\gg\gamma\,,\\ \dfrac{\gamma_0}{(\omega-\omega_0)^2+\gamma_0^2}\,, & \Delta\ll\gamma\,.\end{cases} \tag{86}$$

Here, the first and second Lorentzians correspond to the $0-1$ and $2-3$ transitions, and $\gamma=A$ is the decay rate of state 2. The dynamic theory elaborated in Ref. [82] leads to a similar result. The difference between the two theories shows up in the expression for the half-width γ_0 of the line arising from the $0-1$ transition:

$$\gamma_0=\begin{cases}2f(T)\gamma\,\dfrac{\Delta^2}{\Delta^2+\gamma^2} & \text{(stochastic)},\\ 2f(T)\big[1-f(T)\big]\,\gamma\,\dfrac{\Delta^2}{\Delta^2+\gamma^2} & \text{(dynamic)}.\end{cases} \tag{87}$$

According to expressions (87), the half-width of the $0-1$ line is a nonmonotonic function of the transition rate between the two equilibrium positions; it passes through a maximum at $\gamma=\Delta$, and tends to zero for $\gamma\gg\Delta$.

The shape of the optical band depends strongly on the ratio between the state-2 decay rate γ (Fig. 11b) and the amplitude Δ of the resonance frequency jump. From relationship (86) it follows that the optical band consists of two lines

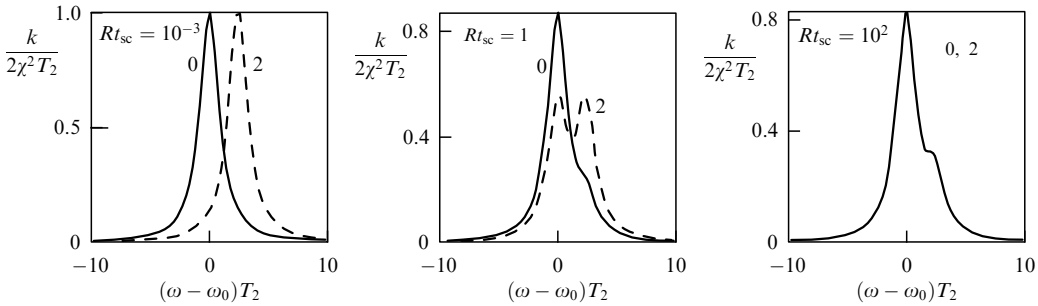

Figure 14. Variation of the optical band shape for a molecule interacting with one TLS versus an increase in laser scan duration; $f = 0.45$, and $\Delta T_2 = 2$. The absorption coefficients k_r (solid curve) and k_b (dashed line) were calculated by formulas (71) and (72) [90, 91].

in the case of infrequent jumps, when the average jump frequency γ is much less than Δ. These two lines are described by Lorentzians with the widths $\gamma_0 \approx 2f\gamma$ and $\gamma_0 + \gamma$, which significantly differ in magnitude only at a low temperature, when $\gamma_0 \ll \gamma$. Conversely, in the case of frequent jumps, when $\gamma \gg \Delta$, the optical band comprises a single line of width

$$\gamma_0 \approx 2f\,\frac{\Delta}{\gamma}\,\Delta = 2f\left(\frac{\Delta}{\gamma}\right)^2 \gamma\,,$$

which is much smaller than the level-2 decay rate γ. In the domain of γ values, where the half-width γ_0 decreases with increasing jump frequency γ, the optical band consists of one line, this line becoming narrower with increasing γ. This effect is referred to as motional narrowing.

From formulas (86) and (87) it follows that, despite the fact that Anderson's stochastic approach [85] invokes the notion of resonance frequency jumps, the absorption coefficient is time-independent and is equivalent to the absorption coefficient in the dynamic theory employing for the TLS an equilibrium density matrix which is time-independent as well. That is why formula (86) cannot describe the absorption coefficient fluctuations observed in SMS on the scale of milliseconds and seconds.

Apart from the works discussed in Section 8, attempts to obtain the time-dependent absorption coefficient were repeatedly made in connection with the problem of spectral diffusion [86–88] in polymers and glass, as well as in connection with the SMS [89]. The dynamic approach considered in Section 8 turned out to be the most effective. That is why our subsequent discussion of the problem of optical band broadening for single molecules relies on the findings of the dynamic theory [90–92].

10.1 Band broadening due to confluence of optical lines

When the frequency separation between two lines emitted by one molecule is smaller than the half-width of each of them, the half-width of the optical band of a single molecule will depend on the laser scan duration in experiment. This situation is illustrated in Fig. 14 corresponding to the case where the chromophore of the impurity molecule interacts with only one TLS, i.e., to the case depicted in Fig. 11b, except that $\Delta < 0$, when the right vertical arrow is longer than the left one and therefore corresponds to the blue line, and the left arrow to the red line. These spectra were calculated in Refs [90, 91] employing two absorption coefficients defined by formulas (71) and (72) for different values of time appearing in these formulas. We showed in Section 9 that these two absorption coefficients may be used for comparison with the averaged absorption coefficients (85) obtained by statistical processing of the fluctuating absorption coefficient found in experiment. The auto- and cross-correlators which are amplitudes in expressions (85) are measured by counting the photon pairs consisting of the r- and b-type photons. However, these measurements may be realized when the red and blue lines are spectrally resolved. In the case depicted in Fig. 14, the lines are poorly resolved, and such a measuring method is inappropriate. How should this situation be treated?

Clearly, the half-width of the optical band may become the measurable quantity in this case. This brings up two questions: first, how should optical band half-width measurements be carried out and, second, what theoretical expression is to be compared with the measured half-width?

Figure 15 depicts the time dependence of the optical band half-width measured by Orrit's group [39] in the following way. The laser frequency was scanned and optical bands were measured in laser scans from the first to the nth. By summation of all the bands they obtained a spectrum averaged over the first n scans. Subsequently, the procedure was repeated for scans from the second to the $(n+1)$, from the third to the $(n+2)$, etc. All spectra averaged over n scans were summed. This double averaging yielded an optical band whose half-width was measured. This half-width is plotted in Fig. 15 as a function of time $t = nt_{sc}$.

According to Fig. 11a, when performing N laser scans we fall fN times on the discrete lower-frequency vertical band which will be referred to as the red trail, i.e., the first emitted

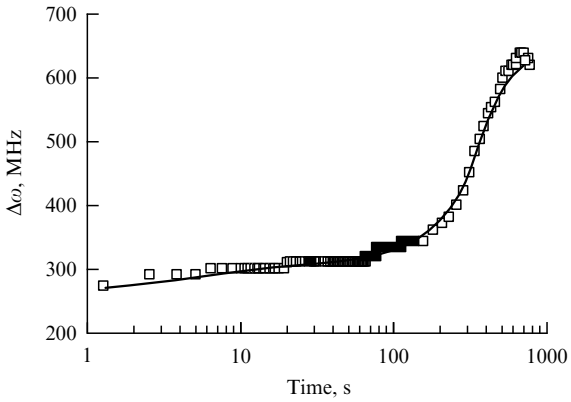

Figure 15. Temporal broadening of the optical band of a terrylene molecule in polyethylene [39] (squares) and the result of a theoretical calculation [90, 91] (curve). Commentary is given in the text.

photon will be of the r-type, and $(1-f)N$ times on the discrete higher-frequency vertical band which will be referred to as the blue trail, i.e., the first emitted photon will be of the b-type. In the former case, by summing all the photons delayed by a time interval nt_{sc} relative to the r-type photon emission time, we measure the absorption coefficient $k_r(nt_{sc},\omega)$ defined by the first of formulas (85), while in the latter case the coefficient $k_b(nt_{sc},\omega)$ defined by the second of formulas (85). In the event of poor line resolution, attempts to separate these two different cases do not meet with success, and, therefore, the absorption coefficient

$$k(nt_{sc},\omega) = k_r(nt_{sc},\omega)\, f + k_b(nt_{sc},\omega)(1-f) \tag{88}$$

is examined in experiment.

On the other hand, the absorption coefficient may be calculated employing formulas (71) and (72), and its half-width may thus be found. In Fig. 15, this half-width for different values of the time is shown with a solid curve which fits the experimental data (squares) quite well.

The above method for the theoretical processing of optical band half-width also applies to more complex cases, when the structure of the optical band is formed due to the interaction with more than one TLS. In the interaction with two TLSs, for instance, two cofactors should be left in the product in formula (63) for the dipole correlator; whence we arrive at the absorption coefficient in the form

$$\begin{aligned} k(\Delta_0,t) = {} & \rho(t)\,\rho'(t)\,L(\Delta_0) + \big(1-\rho(t)\big)\,\rho'(t)\,L(\Delta_0-\Delta) \\ & + \rho(t)\big(1-\rho'(t)\big)\,L(\Delta_0-\Delta') + \big(1-\rho(t)\big)\big(1-\rho'(t)\big) \\ & \times L(\Delta_0-\Delta-\Delta')\,, \end{aligned} \tag{89}$$

where

$$L(\Delta_0) = 2\chi^2\,\frac{1/T_2}{(\omega-\omega_0)^2+1/T_2^2}\,. \tag{90}$$

For short times, i.e., for rapid laser scans, four absorption coefficients result from formula (89) for the four types of initial conditions, and in this case the line jumps from one of four spectral positions to another. In the scanning with intermediate duration, the thermal equilibrium in one TLS manages to set in, with the effect that the dependence on two initial conditions vanishes. In this event, formula (89) generates absorption coefficients of two types. Lastly, the thermal equilibrium manages to settle in both TLSs for long laser scans, and there therefore exists a single absorption coefficient independent of the initial conditions, and the fluctuations of the absorption coefficient are absent.

10.2 Light-induced broadening of lines

Apart from the temporal broadening of the optical bands due to line merging considered in Section 10.1, the line itself of an individual molecule may broaden with time if the intensity of fluorescence-exciting laser radiation is high enough. The dependence of the linewidth of an individual molecule on the excitation intensity was observed by Moerner et al. [36]. The temporal dependence of the light-induced broadening of the optical line emitted by an individual molecule was theoretically analyzed in Ref. [92].

Let us derive a formula that would furnish the description of light-induced broadening of isolated lines. With this in mind we will assume that the local neighborhood contains only one TLS, then this impurity center will possess only two optical lines and will be described by the energy level diagram given in Fig. 11b.

We now consider the case where the light excitation is effected only at the $0-1$ transition frequency. Then, the system of balance equations with the transitions depicted in Fig. 11b takes on the form

$$\begin{aligned} \dot\rho_1 &= -(\Gamma+B)\,\rho_1 + L\rho_0 + b\rho_3\,, \\ \dot\rho_3 &= B\rho_1 - \left(\frac{1}{T_1}+b\right)\rho_3\,, \\ \dot\rho_0 &= \Gamma\rho_1 - (L+a)\,\rho_0 + A\rho_2\,, \\ \dot\rho_2 &= a\rho_0 + \frac{\rho_3}{T_1} - A\rho_2\,, \end{aligned} \tag{91}$$

where $L = k_{0-1}$, and $\Gamma = L + 1/T_1$. The constants describing the transition rates are assumed to satisfy the inequalities

$$\Gamma \gg L \gg A\,, \quad B > a, b, \tag{92}$$

i.e., the frequency of molecular jumps from the ground state to the excited state and back is much higher that the frequency of the tunneling jumps which are indicated by horizontal arrows in Fig. 11b. For this ratio between the constants, the temporal evolution of the probabilities ρ_j experiences two stages — a short and a long one — reflecting the rapid and slow evolution of the ρ_j probabilities, respectively. The rapid evolution occurs in a time on the order of T_1, and to it there corresponds an increase in the probability of finding the molecule in state 1. However, we are concerned with the slow relaxation which occurs upon the establishment of quasi-equilibrium between the populations ρ_1 and ρ_3 of electronically excited states, on the one hand, and the population ρ_0, on the other. The relation between the probabilities in the quasi-equilibrium state can be found by putting $\dot\rho_1 = \dot\rho_3 = 0$. Then, in view of inequality (92), we find the following relationships from the first and second equations:

$$\begin{aligned} \rho_1 &= \frac{(1/T_1+b)\,L\rho_0}{(\Gamma+B)/T_1+b\Gamma} \approx \frac{L}{\Gamma}\,\rho_0\,, \\ \rho_3 &= \frac{BL\rho_0}{(\Gamma+B)/T_1+b\Gamma} \approx \frac{L}{\Gamma}\,T_1 B\rho_0\,. \end{aligned} \tag{93}$$

Substituting the expressions for ρ_1 and ρ_3 into the last two equations of system (91) we arrive at the system of equations

$$\begin{aligned} \dot\rho_0 &= -(\tilde B + a)\,\rho_0 + A\rho_2\,, \\ \dot\rho_2 &= (\tilde B + a)\,\rho_0 - A\rho_2 \end{aligned} \tag{94}$$

which describes the slow relaxation in the impurity center interacting with the TLS. Employing the relationship $\rho_2(t) = 1-\rho_0(t)$, from the system of equations (94) it is easy to obtain the equation

$$\dot\rho_0 = -(\tilde B + R)\,\rho_0 + A \tag{95}$$

comprising the function $\tilde B$, which is a function of the frequency and depends on the laser light intensity. The solution to Eqn (95) equals

$$\rho_0(t) = \frac{A}{\tilde B+R} + \left(\rho_0(0) - \frac{A}{\tilde B+R}\right)\exp\left[-(\tilde B+R)t\right], \tag{96}$$

where

$$\tilde{B} = \frac{L}{\Gamma} B, \qquad R = A + a. \tag{97}$$

According to formulas (93) and (96), the slow relaxation of all populations is determined by tunneling both between states 0 and 2 and between 1 and 3. The transition between states 1 and 3 represents *a light-induced tunneling*. Its rate $\tilde{B}$ is proportional to the pumping L.

As already noted in Section 7.2, in polymers and glass there is a set of TLSs inherent in the solvent (intrinsic TLSs), whose existence is not caused by the presence of an impurity in the polymer. The number of such TLSs is huge and may significantly exceed the number of impurity centers. In such TLSs, the constants b and B of spontaneous tunneling for an excited chromophore are comparable in magnitude to the tunneling constants A and a in the ground electronic state of the chromophore. If the effect of these TLSs is taken into account, the light-induced transitions between states 1 and 3 may be neglected according to formulas (93) and (97), because $L/\Gamma \ll 1$. Such a situation is realized for a chromophore interacting with the TLSs of polymers and glass.

However, the probability of light-induced transitions may exceed the probability of spontaneous ones. This situation prevails in TLSs modeling some transformations in the impurity center, for instance, the attachment of a solvent proton by it. It is precisely these TLSs that participate in the photochemical burning of stable spectral holes in inhomogeneously broadened optical bands. The burning in SMS looks like the disappearance of the optical molecular line for a long time from the spectral region under consideration. These TLSs, as a rule, describe the states of the chromophore itself, i.e., belong to the type of TLSs produced upon introduction of the impurity molecule in the solvent (extrinsic TLSs). Clearly, the number of such TLSs is approximately equal to the number of impurity centers. In the presence of the TLSs produced upon introducing the impurity molecule into the solvent there occurs, as shown by experiment, stable spectral hole burning in the inhomogeneously broadened optical band due to precisely the light-induced tunneling. Since such a hole exists, at low temperatures and when the pump is switched off, for several days or even weeks, this testifies to an extremely low tunneling efficiency in the ground electronic state, i.e., to the smallness of the constants A and a in the extrinsic TLS. Consequently, the light-induced tunneling may not be neglected in these TLSs.

Clearly, the absorption line experimentally found as a result of n laser scans reflects the dependence of fluorescence photon detection probability on the frequency of the exciting laser light. The photon emission probability is proportional to the probability of finding an excited chromophore, i.e., to the probability $\rho_1(t)$, where $t = nt_{sc}$. Employing formulas (93) and (96), for the probability of finding an excited molecule we obtain

$$\rho_1(\Delta, t) = \frac{L}{\Gamma}\left[\frac{A}{\tilde{B}+R} + \left(1 - \frac{A}{\tilde{B}+R}\right)\exp\left(-(\tilde{B}+R)t\right)\right]. \tag{98}$$

Here, use was made of the initial condition $\rho_0(0) = 1$. If $\tilde{B}$ defined by formula (97) is substituted into expression (98), we arrive, in view of

$$L = 2\chi^2 \frac{1/T_2}{\Delta^2 + 1/T_2^2}, \tag{99}$$

at the following expressions for the probability ρ_1 for short and long observation times:

$$\rho_1(\Delta, t) = \begin{cases} \dfrac{L}{\Gamma} \approx 2\chi^2 \dfrac{T_1/T_2}{\Delta^2 + 1/T_2^2}, & t \ll \dfrac{1}{\tilde{B}+R}, \\ 2\chi^2 \dfrac{T_1/T_2}{\Delta^2 + 1/T_2^2(1 + 2\chi^2 T_2 T_1 B/R)}, & t \gg \dfrac{1}{\tilde{B}+R}. \end{cases} \tag{100}$$

The probability (100) is a function of the exciting laser frequency, the passage from the Lorentzian with a half-width $2/T_2$ to the Lorentzian with a larger half-width

$$\Delta\omega_{1/2}(\infty) = \frac{2}{T_2}\sqrt{1 + \frac{2\chi^2 T_2 T_1 B}{R}} \tag{101}$$

taking place for $t \propto 1/(\tilde{B}+R)$. From formula (101) it follows that the maximum half-width value increases as the square root of the excitation intensity, which was observed by Moerner et al. [36]. It was shown in Ref. [92] that formula (101) may be represented as

$$\Delta\omega_{1/2}(\infty) = \frac{2}{T_2}\sqrt{1 + \frac{\tau_{off}}{\tau_{on}(0)}}, \tag{102}$$

and the time interval on which the optical line half-width increases is defined as

$$\frac{1}{\tau} = \tilde{B} + R \approx \frac{1}{\tau_{on}(\Delta)} + \frac{1}{\tau_{off}}. \tag{103}$$

The last two formulas are convenient in that they do not contain unknown parameters, for instance, tunnel transition probabilities. All the quantities that enter into them may be measured in one experiment with relative ease.

Line broadening takes place due to the 'escape' of probability to the off-state. This is evident from formula (102), according to which there occurs no line broadening at $\tau_{off} = 0$, i.e., when the off-state is absent. The role of the 'dark' state is, according to the model considered, played by the TLS state not excited by the laser radiation of the given frequency. Clearly, the role of the dark state can also be played by the triplet molecular state. The triplet broadening mechanism becomes actual for a high probability of the intercombination transition between the singlet and triplet states.

10.3 Temporal broadening of the optical line of an individual molecule caused by interaction with distant two-level systems

There exists one more type of temporal line broadening not discussed above. As already noted, it is possible to derive formula (86) for the time-independent absorption coefficient both in the context of stochastic and dynamic approaches. The difference between these approaches manifests itself only in expression (87) for the optical line half-width. However, unlike the stochastic approach, the dynamic approach allows a simple generalization of formulas (86) and (87) to the case of

a nonequilibrium density matrix for the TLS. It reduces to the replacement of the functions $f(T) = \left[1 + \exp\left(E/k_B T\right)\right]^{-1}$ by the elements $\rho(t, T)$ of the nonequilibrium TLS density matrix in the formulas derived assuming thermal equilibrium. On making this replacement in formula (87) we arrive at the expression

$$\frac{\gamma_0}{2} = \rho(t,T)\big(1 - \rho(t,T)\big)\,\frac{\gamma \Delta^2}{\Delta^2 + \gamma^2} \tag{104}$$

for the optical line half-width caused by the interaction between the chromophore of the molecule and one nonequilibrium TLS. Here $\rho(t, T)$ is described by formula (60). In the framework of the standard TLS model, the interaction between TLSs is neglected. Under these conditions, the contributions of every TLS to the optical line half-width are additive, and the expression for the line half-width assumes the form

$$\frac{\gamma_0}{2} = \sum_j^N \frac{\gamma_j \Delta_j^2}{\Delta_j^2 + \gamma_j^2}\,\rho_j(t,T)\big(1 - \rho_j(t,T)\big)\,, \tag{105}$$

where j is the TLS number. According to formula (104), the contribution of slowly relaxing TLSs to the line half-width is vanishingly small due to the smallness of the value of γ_j which describes the rate of this relaxation. For instance, for a TLS relaxing in 1 s, we arrive at the expression for the contribution to the line half-width: $\gamma_0 \propto \gamma = 1\ \mathrm{s}^{-1}$, which is ten orders of magnitude smaller than the experimentally examined half-width. However, according to the standard TLS model proposed by Anderson et al. [37], the distribution of the TLSs over the relaxation constants is hyperbolic, i.e., $N(\gamma) \propto 1/\gamma$. This signifies that the slowly relaxing TLSs far outnumber the fast-relaxing ones. Although the contribution of a slow-relaxing TLS to the line half-width is small, such TLSs are great in number and their integral contribution is therefore noticeable.

From the stochastic theory [88] and formula (105) of the dynamic theory [93] it follows that the line half-width depends linearly on the temperature T, and logarithmically on the time:

$$\gamma_0 = \frac{1}{T_2} \propto k_B T \log\left(R_{\max} t\right), \tag{106}$$

if the TLS – chromophore interaction is of the dipole – dipole type. Here $R_{\max}$ is the highest TLS relaxation rate.

The logarithmic dependence on the 1-to-100 s time interval is evident, for instance, from the experimental data given in Fig. 15. Only when the logarithmic dependence in theoretical formulas is taken into account can the calculated curve be fitted with experimental points. The logarithmic temporal line broadening also shows up in an AF fluorescence experiment. This issue will be discussed in greater detail in Section 11.

However, the predictions of stochastic and dynamic theories diverge significantly for a different chromophore – TLS interaction type. The stochastic theory predicts a non-Lorentzian line profile, while the dynamic theory predicts the Lorentzian profile but a different temporal behavior of the line half-width. This behavior depends on the rate of spatial weakening of the above chromophore – TLS interaction. It was shown in Ref. [93] that the form of the temporal dependence of the optical line half-width depends on the type of electrostatic chromophore – TLS interaction. For a dipole – quadrupole interaction, one finds $\gamma_0 \propto 1 - (R_{\max} t)^{-1/4}$, while for a dipole – monopole interaction $\gamma_0(t) \propto (R_{\max} t)^{1/2} - 1$. So far, both dependences have been observed only in experiments involving spectral hole burning, specifically the half-widths of spectral holes which were burned in these experiments in an inhomogeneously broadened optical band [94, 95].

It is pertinent to note that formula (105) describes only the TLS's contribution to the half-width. In a real solvent, there is always an interaction between the impurity molecule and phonons. That is why the experimentally found PLL half-width is expressed in the following form

$$\Delta\omega_{1/2} = \frac{2}{T_2} = \gamma_0(t,T) + \gamma_{\mathrm{ph}}(T)\,, \tag{107}$$

where the second term on the right-hand side describes the contribution of electron – phonon interaction to the half-width. The contribution from phonons is time-independent, because phonons are rapidly relaxing quasiparticles. For a temperature of 4.2 K and lower, the contribution to a PLL broadening is made primarily by TLSs. However, the contribution from phonons begins to prevail with increasing temperature. This fact was established in photon echo experiments [84].

11. Diversity of the optical bands of individual impurity centers

The inhomogeneous broadening of the optical bands from impurity centers in polymers and glass, which typically exceeds 100 cm^{-1}, has commonly been attributed to the fact that the local environment of individual impurity centers in these matrices varies from center to center, which is responsible for the spread in their resonance frequencies.

Even in their first works on single molecules, Moerner's group [35, 96] demonstrated that the resonance frequency jumps of individual impurity centers, occurring on a scale of several thousand seconds, i.e., the quantum trajectories of the resonance frequency, vary strongly in going from center to center. In other words, the resonance frequency fluctuations of individual impurity molecules are also individual. However, at that time it was not yet clear how to extract the information about the local environment from the quantum frequency trajectories.

The next step was made by Orrit's group [97] which investigated not the fluctuations but the autocorrelation functions of individual molecules, which are related by simple formulas (54) to the probability of observing photon pairs separated by a time interval Δt. It turned out that the AFs of individual impurity centers were also individual; an example of this kind is given in Fig. 16. The AF is conveniently plotted on a logarithmic time scale, for it permits us to demonstrate in one drawing the relaxation effects described by exponential functions with characteristic times varying by orders of magnitude. Here, the weak logarithmic time dependence of the AF arises from the logarithmic time dependence of the optical dephasing rate $1/T_2$, considered in Section 10. As we saw in the consideration of the AF for a molecule with a triplet level, the smoothed AF step, which occupies one order of magnitude on the time scale, corresponds to the exponential relaxation in going from the singlet system to the triplet one. The TLS relaxation is also described by an exponential function. Curve *1* in Fig. 16 exhibits two such smoothed steps, while curves *2* and *3* show

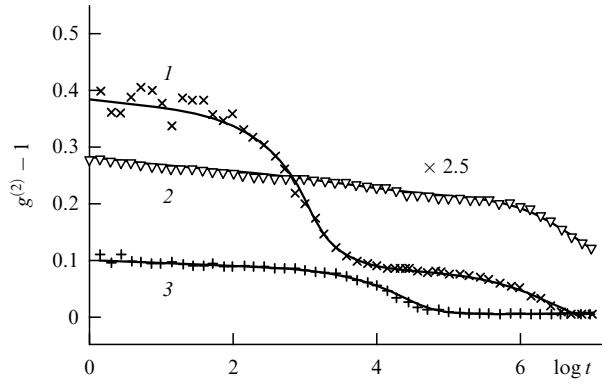

Figure 16. Autocorrelation function of three individual terrylene molecules in polyethylene at $T = 1.8$ K (symbols) [97]. Theoretical dependences (solid curves) were calculated in Ref. [47]. The time t is measured in microseconds.

one step each. This signifies that impurity center *1* obeys a biexponential relaxation law, while impurity centers *2* and *3* obey monoexponential laws, their relaxation constants differing by two orders of magnitude. In this case, we are dealing with the relaxation of TLSs strongly coupled to the impurity center, i.e., resided in its local environment. The question of how it is possible to judge the microscopic impurity center model from the AF form is considered in greater detail in Refs [57, 63, 64].

At present, it is valid to say that two avenues of SMS development exist. Works pursuing the first line study the dynamics of individual molecules, which manifest themselves in the time dependence of the measurement data. Works of this kind were discussed in Sections 3–10. Work along the second line involves statistical processing of the experimental data obtained in the investigation of several hundred individual molecules but for a fixed measuring time. Belonging to the latter are Refs [69, 78, 97–101] which were concerned with the statistical processing of experimentally obtained optical bands of several hundred individual molecules.

The first finding resulting from this statistical processing was the distribution functions of the optical band half-widths of individual molecules [97, 98]. The band half-width was measured for a fixed time. Such a distribution is exemplified in Fig. 17e. In Sections 10.1–10.3, we considered three types of optical band broadening. The distribution in Fig. 17e was plotted for the widths discussed in Section 10.1. Distributions of this kind were measured in Ref. [98] for terrylene molecules in different polymer matrices and even in an anthracene single crystal. The latter signifies that a discrete set of local environments in which a foreign molecule may find itself exists even in a single crystal.

The half-width averaged over this distribution was found to be in satisfactory agreement with the half-width of spectral holes burned in the same matrices. The question of what half-width is measured in echo experiments was also cleared up. Vainer et al. [101] discovered that the smallest widths of these distributions correspond to the optical dephasing rate $1/T_2$ measured in photon echo experiments. These width distributions were also found to shift to the right with increasing temperature, which is attributable to temperature line broadening.

The above examples demonstrate that the analysis of linewidth distributions for individual molecules, i.e., the actual second moments of the optical bands, allowed the solution of several problems hotly debated prior to the advent of SMS. That is why a group of Russian and German researchers [78, 99, 100] proceeded further along this path and measured the distribution functions for the moments

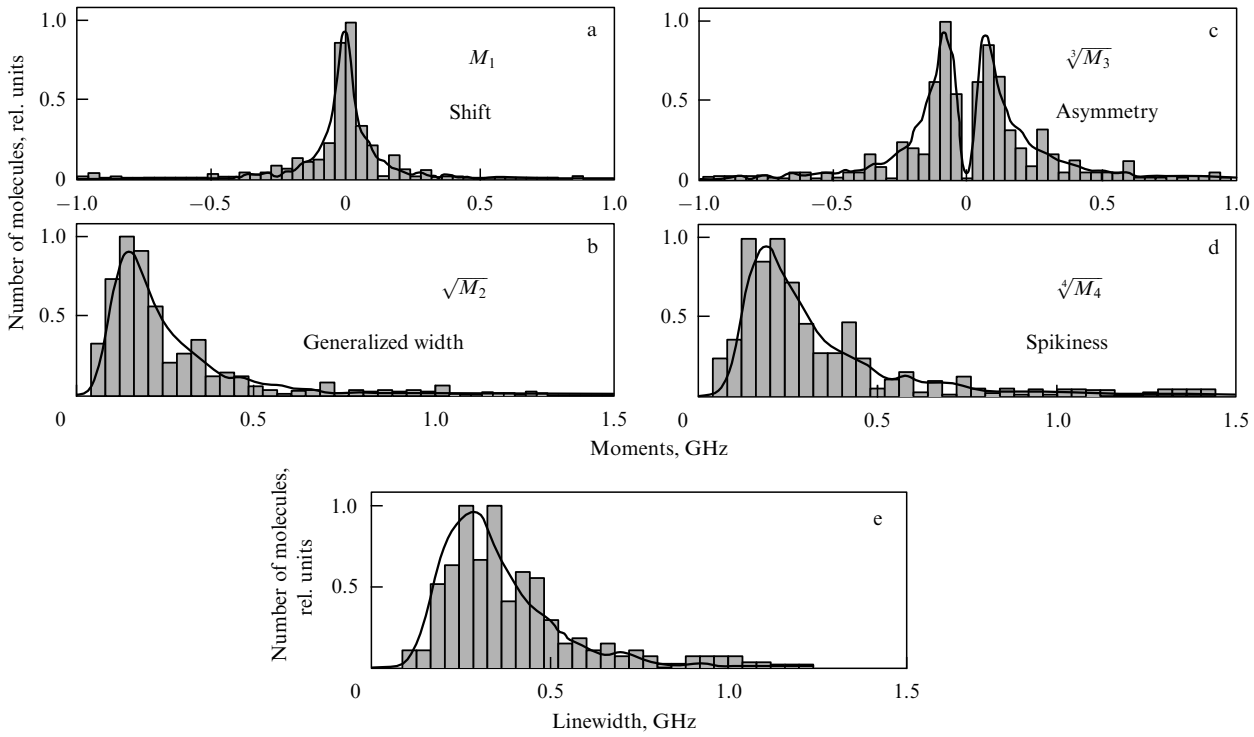

Figure 17. Distribution of the first moments of the optical bands of individual tetra-*tert*-butyl terrylene molecules introduced into the polyisobutylene polymer matrix at $T = 2$ K [78, 99, 100].

from the first to the fourth for several hundred individual tetra-*tert*-butyl terrylene molecules introduced into a polymer polyisobutylene matrix. These experimental data are given in Fig. 17.

On the other hand, by setting, say, one hundred times the random parameter distributions of TLSs interacting with an impurity molecule it is possible to obtain with the aid of theory [67, 68] one hundred sets of optical bands and to construct the theoretical curves for the moments. The curves in Fig. 17 were calculated employing the Geva – Skinner theory [67, 68].

When discussing the Geva – Skinner theory in Section 9, we noted as a drawback the poor description of the temporal behavior of the optical bands from individual molecules. However, this drawback does not affect the calculated shape of the optical band, when the measuring time is far longer than the relaxation times of all the TLSs from the closest environment of the chromophore. In this case, all the TLSs of the local environment are in a state of thermal equilibrium, and the Geva – Skinner theory adequately takes into account the effect of the thermally equilibrium TLSs on the optical band. Since the distributions plotted in Fig. 17 were measured under precisely this condition, satisfactory agreement between the theoretical and experimental results in Fig. 17 is hardly surprising despite the drawbacks of the theory relating to the description of the local dynamics of individual molecules. These drawbacks of the Geva – Skinner theory supposedly cannot manifest themselves in such averaged characteristics as optical band moments.

The characteristic which relates to the fourth moment and was termed 'spikiness' by the authors of Ref. [78] was investigated more recently by the same authors [100]. In this work, they measured the ratio between the number of optical bands unsplitted into lines and the number of observed doublets, quadruplets, etc. The authors established that the theory which takes into account the dipole – dipole nature of the interaction between the chromophore of the impurity molecule and the TLS is capable of reproducing the experimentally examined ratio between the number of doublets and the number of single lines, this being so only for a certain value of the minimal distance between the impurity molecule and the nearest TLS, which turned out to be equal to about 2 nm. Clearly, this is the average distance value.

During the early years of developing the low-temperature SMS, verification and refinement of the TLS model proposed by P Anderson et al. [37, 38] for the description of low-temperature anomalies of glass became one of the main areas of SMS studies. This model had previously proved to be efficient in many nonoptical low-temperature experiments performed on glass. In optical experiments, this model was widely used for describing impurity centers in polymers. The interaction between the chromophore of an impurity molecule and a TLS had to give rise to optical line doublets and to optical bands with a more complex shape, which had not been observed prior to the advent of SMS. The spectra of single molecules removed any doubt which might have remained regarding the TLS model. At the same time, SMS provided a wealth of exemplifying spectra which defy explanation by the standard TLS model.

The trails of individual molecules, similar to those shown in Fig. 11a, might serve as a tool for the verification of the TLS model. Although this model had been introduced three decades prior to the commencement of investigations of single molecules, it continued to raise numerous discussions due to its phenomenological nature and the lack of convincing theoretical substantiation. The time-dependent trails characterizing the dynamics of individual molecules, which were measured by Orrit's group [39] for many individual molecules, yielded much new information on the TLS model.

Boiron et al. [39] measured the trails of 70 individual terrylene molecules in a purely amorphous polyisobutylene polymer and of 14 terrylene molecules in a semicrystalline polyethylene polymer at a temperature of 1.8 K. Both polymers were nonpolar. From the trails it was established that the optical bands of 70% of the molecules correspond to the bands predicted by the standard TLS model. In view of this fact, it becomes clear why the experimental data obtained by the method of spectral hole burning are well described by the TLS model. Manifested in this method are ensembles of the molecules with one and the same resonance frequency, and the dynamics of the majority of impurity centers of an ensemble is, as evidenced by the data of Ref. [39], described by the TLS model.

Of those centers whose dynamics were described by the TLS model, 40% possessed an optical band consisting of one optical line, another 40% possessed optical bands consisting of line doublets, 16% exhibited an optical band comprising line quadruplets, and all the remaining cases accounted for closing 4%. Among the spectra of individual molecules measured in Ref. [39], 30% contained trails which could not be described by the standard TLS model.

12. Fluorescence fluctuations of single polymer molecules

As noted in Section 2, since the mid-1990s it has become apparent that SMS techniques are effective at room temperature, too. Single-molecule spectroscopy permits the investigation of the dynamics of a complex quantum system at room temperature, because in SMS, along with spectroscopic studies traditional for molecular ensembles, it is also possible to measure the fluorescence fluctuations, which underlies the efficiency of room-temperature SMS. This is a circumstance of great significance, since such objects as the light-harvesting systems of photosynthesis centers, proteins, and other biologically active molecules function in living organisms at room temperature.

This brings up the natural question of what we must bear in mind while on the subject of a single molecule. Why, for instance, do ten anthracene molecules (chromophores) dissolved in a polymer behave like a molecular ensemble with a nonfluctuating fluorescence and therefore yield little information at room temperature, whereas a polymer chain comprising a hundred chromophores and possessing an atomic weight above 20,000 a.m.u. may be treated as a single molecule, as evidenced by its fluctuating fluorescence?

When answering this question we are reminded that a single molecule in SMS is irradiated by the light of a cw laser and the information about the molecular dynamics is extracted by counting the fluorescence photons. Early in SMS development, investigations were made of molecules with one chromophore: such molecules are unable to absorb the second photon prior to the emission of the previously absorbed photon. Such a single molecule may be termed a single absorber and single emitter of photons. However, polymer molecules and light-harvesting antennas of photosynthesis centers exhibit exciton type absorption [102]. This

signifies that light is simultaneously absorbed by many chromophores and therefore the simultaneous absorption of two or more photons with the production of two or more excitons is possible, i.e., in the latter case the single molecules are no longer single absorbers.

Clearly, for a low light intensity, the probability that there exists one exciton in a single molecule will prevail even in polyatomic light absorption, of which exciton absorption is one type. Therefore, despite the polyatomic nature of the absorption, the emission retains its single-photon nature. This circumstance is of decisive importance for the emergence of fluorescence fluctuations.

By a specific example, we will show how the theory may be applied in the analysis of experimental data in the case of fluctuating fluorescence of complex molecules. This was demonstrated in Ref. [103]. For the experimental material, advantage was taken of the data on the fluorescence of a single PPV – PPyV copolymer molecule, obtained by Barbara's group [12].

12.1 Experimental data

Spectroscopic investigations of the ensembles of polymer molecules reveal that light is absorbed by a set of polymer chromophores, and that emission occurs upon electronic energy migration to the local minima of the potential Frank – Condon surface in a polymer molecule [104]. For instance, in a polymer in which anthracene molecules were used as pendants to the polymer chain, the emission took place from anthracene molecules located at the ends of the polymer chain [105]. Unfortunately, it is impossible to separate the intermolecular energy transfer from the intramolecular one in molecular ensembles. That is why the Barbara group undertook a number of studies of the energy transfer in single PPV – PPyV copolymer molecules in which the electronic energy transfer is known to be an intramolecular process. The energy transfer was examined by observing the fluorescence of individual molecules of this polymer.

The molecular weight of the molecules under investigation was equal to about 20,000 a.m.u., i.e., they contained 80 – 100 chromophores capable of absorbing light. Figure 2 portrays the absorption and emission bands of this polymer. Since the optical polymer bands are structureless, information about polymer dynamics cannot be extracted from them. The fundamental difference between the fluorescence of a single polymer molecule and the fluorescence of an ensemble manifests itself in the temporal fluorescence behavior. The fluorescence intensity of the ensemble of polymer molecules is time-independent, while the fluorescence intensity of a single molecule fluctuates, as shown in Fig. 3. The fluorescence signal was accumulated within the span of 0.1 s. The character of the fluorescence QIT was shown to remain invariable under excitation by $\lambda = 514$ nm light.

Van den Bout et al. [12] performed a statistical QIT processing for several dozen single polymer molecules. Their results are presented in Fig. 18. These data suggest that the fluorescence intensity of every single polymer molecule flickers, i.e., it now emerges (on-intervals), now vanishes (off-intervals). The on-interval fluorescence may have two intensity levels: I_1, conventionally termed average, and the high level I_2, i.e., the fluorescence is binary in intensity. The on-interval duration depends on the excitation intensity, while the off-interval duration does not. The data given in Figs 2, 3, and 18 underlie the theoretical model considered in next Section 12.2.

12.2 Theoretical model

The theoretical model should describe both the double level of fluorescence intensity and its blinking, i.e., the existence of the on-intervals, as well as of the off-intervals.

Model with a double fluorescence intensity. We are reminded that the fluorescence with two intensity levels has been observed not only for a single polymer molecule. For instance, the fluorescence of a single tetra-*tert*-butyl terrylene molecule introduced into polyisobutylene, shown in Fig. 11a, also exhibits two intensity levels. The theoretical model invoked to explain this fluorescence takes into account the interaction between the chromophore of the molecule and the TLS of the polymer matrix. Modelled with the aid of the TLS is the conformational change in the impurity complex consisting of the impurity molecule and the closest polymer molecular environment. Since the absorption at the $1-0$ and $3-2$ transition frequencies is different, the fluorescence intensities are also different, i.e., we are faced with two fluorescence intensity levels. The ratio between the integral values of the two fluorescence intensities for a long scanning time is equal to the ratio between the peak values of the curves in Fig. 13b.

Blinking fluorescence model. The model considered above cannot explain the disappearance of fluorescence at certain instants of time, i.e., the occurrence of off-intervals. This can be done with another model represented in Fig. 7 which depicts the energy level diagram comprising two singlet levels and one triplet level. This diagram is typical of organic molecules. Such a molecule fluoresces during the on-intervals interrupted by off-intervals, when there is no fluorescence. This model was discussed in detail in Section 7.

Model reproducing the fluorescence dynamics of a polymer chain. This is a combination of the two models considered above. The key elements allowing one to construct the physical polymer model capable of reproducing the QIT depicted in Fig. 3 are as follows:

(i) the existence of three fluorescence intensity levels: zero, medium, and high (Fig. 18);

(ii) accounting for the fact that jumps from the medium fluorescence level I_1 to the high level I_2 and back take place, as a rule, when the intensity drops to zero (see Fig. 3);

(iii) the reverse on-interval duration which depends linearly on the excitation power, and the power-independent off-interval duration;

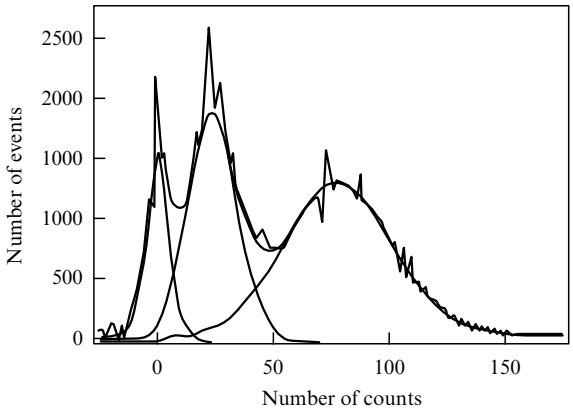

Figure 18. Three fluorescence intensity levels of single molecules: zero, medium I_1, and high I_2, with the respective count rates of 0, 25, and 75 [12].

(iv) the glow-interval (on-interval) and non-glow-interval (off-interval) durations belonging to a time scale of seconds (see Fig. 3).

A polymer chain along which N light-absorbing chromophores are located at regular intervals offers a model of a one-dimensional crystal. Clearly, the three levels depicted in Fig. 7 may correspond to every chromophore. Owing to the interaction between the chromophores, N excited singlet levels make up a singlet exciton band responsible for light absorption by the polymer, and $3N$ triplet levels form a triplet exciton band; when the polymer finds itself in the triplet exciton band, it does not radiate.

The interaction between the solvent molecules and the polymer chromophores will result in the emergence of defect levels below the bottom of the singlet band and the bottom of the triplet band; singlet or triplet electronic excitations may end up in these levels. The defect levels play the part of traps for electronic excitation. The shape of the fluorescence bands of shallow traps and its dependence on the temperature and trap depth were considered in Refs [81, 106].

Strictly speaking, several defect levels, i.e., traps, may be located below the bottom of the singlet exciton band. However, the clearly defined fluorescence intensity fluctuations with drops to zero, which are depicted in Fig. 3, are an indication that the polymer molecule emits photons from a single channel whose role is supposedly played by the lowest defect level. It would therefore be sufficient to include only one defect level. Indeed, if there were two independent emitters, the radiation picture would result from the summation of two QITs, similar to the QIT depicted in Fig. 3, with a random shift on the time scale. Clearly, the new QIT resulting from the summation would possess more fluorescence intensity levels than we see in Fig. 18.

The existence of an exciton band and defect levels, which play an important part in luminescence kinetics, will hardly affect the shape of an absorption band and fluorescence at room temperature. The Gaussian shape of the bands in Fig. 2 suggests that the strong electron – phonon interaction 'hides' the electronic level structure caused by the exciton band and the defect level. In the case of impurity centers with a strong electron – phonon interaction, the absorption and fluorescence bands depicted in Fig. 2 may therefore be described by the following functions [11]

$$I^{\mathrm{a,e}}(\omega) = \frac{1}{\sqrt{2\pi D}} \exp\left(-\frac{(\omega - \omega_0 \mp C)^2}{2D}\right). \qquad (108)$$

Here, the Stokes shift $2C$ and the half-width $\Delta\omega_{1/2} = \sqrt{2D\ln 2}$ of the bands are defined by the formulas

$$C = \sum_{q=1}^{N_0} \frac{a_q^2}{2} v_q\,, \qquad D = \sum_{q=1}^{N_0} \frac{a_q^2}{2} v_q^2 \coth\left(\frac{\hbar v_q}{2k_{\mathrm{B}}T}\right), \qquad (109)$$

where v_q and a_q are the normal vibration frequencies of the polymer molecule and the shifts of the equilibrium positions of the normal coordinates, respectively, and T is the temperature of the sample.

In accordance with the aforesaid, the energy diagram of a polymer molecule may be represented in the form shown in Fig. 19. According to this diagram, the polymer molecule possesses two conformations, to which there correspond levels 0, 1, 2 and $0'$, $1'$, $2'$. The energies of 1 and $1'$ levels correspond to the singlet exciton and the singlet trap in these conformational forms. Two fluorescences with different

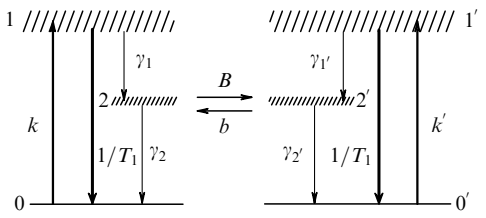

Figure 19. Energy diagram of a PPV – PPyV polymer molecule subjected to conformational changes in the triplet state.

intensity levels are clearly relevant to transitions from states 1 and $1'$ to the ground state. The energies of 2 and $2'$ correspond to the triplet exciton and the triplet trap. Without an assumption that there occur jumps of the polymer molecule from one conformational form to the other, it is impossible to explain the existence of fluorescence with two intensity levels, and without the inclusion of triplet states it is impossible to account for the emergence of the off-intervals.

We have tried to represent the magnitude of the probabilities for transitions indicated by arrows via their thickness: the thicker the arrow, the higher the transition probability. Therefore, we make use of the following hierarchy of relaxation constants:

$$\frac{1}{T_1} \gg k, k' \gg \gamma_2, \gamma_{2'}, \gamma_1, \gamma_{1'}, B, b\,. \qquad (110)$$

The absence of stimulated fluorescence in the diagram drawn in Fig. 19 is attributable to the fact that light absorption is effected by excitons whose energy thermalization time is shorter than the duration of a fluorescence event. Under these conditions there is no resonance fluorescence.

It is evident that the conformational change on the time scale of seconds may occur either in the ground state or in the long-lived triplet state of a polymer molecule. If the conformational change occurred in the ground electronic state, the medium-to-high fluorescence level transition of the system would take place in jumps without reaching the off-state. This is at variance with the fact that the jumps from the medium fluorescence level to the high level and back take place after the intensity drops to zero. That is why we showed in the diagram in Fig. 19 that the conformational change occurs when the polymer molecule finds itself in the triplet state of the trap.

The balance equations for the probabilities of finding a polymer molecule in one of the six quantum states represented in Fig. 19 take on the following form:

$$\begin{aligned}
\dot\rho_1 &= -\left(\frac{1}{T_1} + \gamma_1\right)\rho_1 + k\rho_0\,,\\
\dot\rho_0 &= \frac{\rho_1}{T_1} - k\rho_0 + \gamma_2\rho_2\,,\\
\dot\rho_2 &= \gamma_1\rho_1 - (\gamma_2 + B)\rho_2 + b\rho_{2'}\,,\\
\dot\rho_{1'} &= -\left(\frac{1}{T_1} + \gamma_{1'}\right)\rho_{1'} + k'\rho_{0'}\,,\\
\dot\rho_{0'} &= \frac{\rho_{1'}}{T_1} - k'\rho_{0'} + \gamma_{2'}\rho_{2'}\,,\\
\dot\rho_{2'} &= B\rho_2 + \gamma_{1'}\rho_{1'} - (\gamma_{2'} + b)\rho_{2'}\,.
\end{aligned} \qquad (111)$$

The meaning of all constants is evident from Fig. 19. System of equations (111) describes both the fast relaxation taking a course on the T_1-time scale and the slower relaxation occurring on the time scale of singlet – triplet transitions and of the transitions from one conformation to the other. In the experiment under discussion, the information about the fast relaxation was lost due to the insufficient temporal resolution of the facility, which allowed measuring only the slow relaxation. If we are concerned with only the slow relaxation in the polymer molecule, system of equations (111) may be simplified as follows. We put $\dot\rho_1 = \dot\rho_{1'} = 0$. Then, from the first and fourth equations of system (111) we find that

$$\rho_1 = \frac{kT_1}{1+\gamma_1 T_1}\,\rho_0\,, \qquad \rho_{1'} = \frac{k'T_1}{1+\gamma_{1'}T_1}\,\rho_{0'}\,. \tag{112}$$

Substituting these expressions into the remaining four equations we arrive at the system of equations

$$\begin{aligned}
&\dot\rho_0 = -k_e\rho_0 + \gamma_2\rho_2\,,\\
&\dot\rho_2 = k_e\rho_0 - (\gamma_2 + B)\,\rho_2 + b\rho_{2'}\,,\\
&\dot\rho_{0'} = -k'_e\rho_{0'} + \gamma_{2'}\rho_{2'}\,,\\
&\dot\rho_{2'} = k'_e\,\rho_{0'} + B\rho_2 - (\gamma_{2'} + b)\,\rho_{2'}\,,
\end{aligned} \tag{113}$$

where

$$k_e = \frac{\gamma_1 T_1}{1+\gamma_1 T_1}\,k\,, \qquad k'_e = \frac{\gamma_{1'}T_1}{1+\gamma_{1'}T_1}\,k' \tag{114}$$

describe the effective rate of triplet states pumping via excited singlet states in both conformational forms. System of equations (113) governs the slow relaxation of the system involved, which proceeds upon rapid population of levels 1 and $1'$ and enables the calculation of the on- and off-interval distributions in duration, as well as the determination of the average durations of these intervals. Since the polymer molecule can reside in two fluorescing conformational forms, we should observe in its fluorescence two types of on-intervals and two types of off-intervals.

12.3 Autocorrelation function

The fluorescence intensity is proportional to the effective absorption coefficients which describe not only the exciton absorption but also comprise the rate of energy transfer from a polymer molecule to the luminescent trap. Since the polymer molecule executes quantum jumps from one conformation to the other, the effective absorption coefficient will fluctuate. By measuring the fluctuating fluorescence QIT, it is possible to construct the AF

$$g^{(2)}(\tau) = \lim_{t\to\infty}\frac{\langle I(t)\,I(t+\tau)\rangle}{\langle I(t)\,I(t+\infty)\rangle} = \lim_{t\to\infty}\frac{\langle I(t)\,I(t+\tau)\rangle}{\langle I(t)\rangle^2}\,, \tag{115}$$

where $I(t)$ is the fluorescence QIT. According to formula (115), to measure the AF requires shifting the QIT by a time τ relative to itself and count the number of photon pairs with the given time delay, which will be proportional to the QIT length and the degree of on-intervals coincident in the two QITs shifted by the time τ relative to each other.

This brings up the question: how is it possible to theoretically evaluate the AF? As shown in Section 7, the AF is related to the full two-photon correlator $p(\tau)$ by the simple formula

$$\frac{p(\tau)}{p(\infty)} = g^{(2)}(\tau)\,.$$

The full two-photon correlator, which is defined as the counting rate for the photon pairs separated by a time interval τ, may be calculated for a given microscopic model of the radiating system. When there is only one fluorescent state, the full two-photon correlator is defined as

$$p(\tau) = \frac{\rho_1(\tau)}{T_1}\,, \tag{116}$$

where $\rho_1(\tau)$ is the probability that the system is found in the fluorescent state at the expiration of the time τ after the instant it emits a photon. For a molecule with the system of energy levels depicted in Fig. 19, it is easily found that $\rho_1(\tau) \approx kT_1\,\rho_0(\tau)$ for $kT_1 \ll 1$, and therefore

$$p(\tau) \approx k\rho_0(\tau)\,, \tag{117}$$

i.e., the two-photon correlator is proportional to the absorption coefficient; therefore, the fluorescence intensity will be proportional to the correlator. However, in our case there are two fluorescent states 1 and $1'$, and, therefore, two types of fluorescence with intensities I_1 and I_2. And therefore the question arises: what probabilities should the expression for the two-photon correlator comprise?

We assume for definiteness that the fluorescence with intensities I_1 and I_2 relates to the states 1 and $1'$, respectively. Let us assume that the fluorescence with the intensity I_2 is artificially removed from the measured QIT, and only the fluorescence with the intensity I_1 is retained. Then, $I = I_1$ and we arrive at the following expression

$$g_1^{(2)}(\tau) = \lim_{t\to\infty}\frac{\langle I_1(t)\,I_1(t+\tau)\rangle}{\langle I_1(t)\rangle^2} = \frac{p(\tau)}{p(\infty)}\,, \tag{118}$$

where the two-photon correlator $p(\tau)$ is defined by formula (36). If, conversely, only the fluorescence with the intensity I_2 is kept in the QIT, then one has

$$g_2^{(2)}(\tau) = \lim_{t\to\infty}\frac{\langle I_2(t)\,I_2(t+\tau)\rangle}{\langle I_2(t)\rangle^2} = \frac{p'(\tau)}{p'(\infty)}\,, \tag{119}$$

where

$$p'(\tau) = \frac{\rho_{1'}(\tau)}{T_1}\,. \tag{120}$$

The probabilities $\rho_1(\tau)$ and $\rho_{1'}(\tau)$ can be calculated with the aid of formulas (112), and then the expressions for the correlators take on the form

$$\begin{aligned}
&p(\tau) = \frac{k}{1+\gamma_1 T_1}\,\rho_0(\tau) \approx k\rho_0(\tau)\,,\\
&p'(\tau) = \frac{k'}{1+\gamma_{1'}T_1}\,\rho_{0'}(\tau) \approx k'\rho_{0'}(\tau)\,,
\end{aligned} \tag{121}$$

i.e., in this case there are two types of two-photon correlators and, consequently, two absorption coefficients and two fluorescence types, because

$$p(\tau) \propto I_1(\tau)\,, \qquad p'(\tau) \propto I_2(\tau)\,. \tag{122}$$

The probabilities $\rho_0(\tau)$ and $\rho_{0'}(\tau)$ are found from the system of equations (113) subject to the initial conditions $\rho_0(0) = 1$ and $\rho_{0'}(0) = 1$, respectively.

Formulas (121) define the intensities of two types of fluorescence. The time dependence of fluorescence intensity is determined by the time dependence of the probability that a molecule is found in the ground state with one conformation or the other.

The numbers of fluorescence photons counted during a time interval t are expressed as

$$N_1(t) = \int_0^t p(\tau)\,\mathrm{d}\tau\,, \qquad N_2(t) = \int_0^t p'(\tau)\,\mathrm{d}\tau\,, \tag{123}$$

while the fluorescence intensities measured in experiment are calculated from the relationships

$$I_1 = \frac{N_1(t)}{t}\,, \qquad I_2 = \frac{N_2(t)}{t}\,. \tag{124}$$

These intensities as functions of the photon counting time t were calculated by formulas (121) in Ref. [103]. For an acquisition interval of 0.1 s employed in Ref. [12], the fluorescence intensity fluctuates between the two values I_1 and I_2 indicated in Fig. 18. The ratio between these two intensity values is equal to 1/3, i.e., to the ratio 25/75 — the numerator and the denominator in the fraction correspond to the positions of the two peaks in Fig. 18. The average decay time of the excited singlet state to the triplet state was found to be equal to about 0.1 s, and the average time of decay of one polymer molecule conformation, involving transition to the other, to about 12 s [103].

12.4 On- and off-interval distributions

With the aid of system of equations (113), it is also possible to find the functions defining the on-interval distribution in duration. These functions are of the exponential form:

$$\begin{aligned} w_{\mathrm{on}}^{(1)}(t) &= \frac{1}{\tau_{\mathrm{on}}^{(1)}} \exp\left(-\frac{t}{\tau_{\mathrm{on}}^{(1)}}\right), \\ w_{\mathrm{on}}^{(2)}(t) &= \frac{1}{\tau_{\mathrm{on}}^{(2)}} \exp\left(-\frac{t}{\tau_{\mathrm{on}}^{(2)}}\right), \end{aligned} \tag{125}$$

where

$$\begin{aligned} \frac{1}{\tau_{\mathrm{on}}^{(1)}} &= \frac{\gamma_1 T_1}{1 + \gamma_1 T_1 + k T_1}\, k\,, \\ \frac{1}{\tau_{\mathrm{on}}^{(2)}} &= \frac{\gamma_{1'} T_1}{1 + \gamma_{1'} T_1 + k' T_1}\, k'\,. \end{aligned} \tag{126}$$

It is evident from these results that the on-interval distributions with different fluorescence intensity levels I_1 and I_2 may be described by exponential functions with different exponents. Had the on-interval distributions with different fluorescence intensity levels been separately measured, from the experiment we would have directly found $\tau_{\mathrm{on}}^{(1)}$ and $\tau_{\mathrm{on}}^{(2)}$. They now have a simple physical significance: these times determine the average duration of the on-intervals with moderate and bright fluorescence. However, van den Bout et al. [12] measured the total on-interval distribution in duration:

$$w_{\mathrm{on}}^{(1)}(t) + w_{\mathrm{on}}^{(2)}(t)\,, \tag{127}$$

whence it follows that the reciprocal of the average on-interval duration is a linear function of excitation intensity. This is in perfect agreement with formulas (126), when taken into account that $kT_1 \ll 1$ and $k'T_1 \ll 1$. The dependence of the on-interval duration on the light pump also testifies to the fact that conformational changes occur in the triplet state. Were it occurring in the ground state, the on-interval duration would be independent of the light pump intensity.

By using the experimentally determined average on-interval duration and the simplified formula

$$\frac{1}{\tau_{\mathrm{on}}} \approx \gamma_1 T_1 k = \frac{1}{150}\ \mathrm{ms}^{-1}\,, \tag{128}$$

we can estimate the intercombination transition rate γ_1 for this polymer. According to Ref. [12], approximately 4000 photons per second are recorded with a PM in the measurement of single-molecule fluorescence. For a quantum fluorescence photon detection efficiency of 10^{-3} and a quantum yield of fluorescence of about 0.1, we obtain that $k = 4000 \times 10^3 \times 10 = 4 \times 10^7\ \mathrm{s}^{-1}$. Substituting this value into the approximate formula (128) we obtain, for $T_1 = 10^{-9}$ s, the value of the intercombination transition probability in the polymer molecule $\gamma_1 = 1.6 \times 10^2\ \mathrm{s}^{-1}$, i.e., the singlet – triplet transition is 10^6 times less probable than the singlet – singlet transition.

To summarize the aforesaid, we can draw the following conclusion. Processing the fluctuating fluorescence data from Ref. [12] with the aid of the theory of light absorption by single molecules has allowed us to construct a theoretical model [103] for the description of electronic excitation energy transfer in a single polymer molecule to the fluorescent center of this molecule, and to determine the magnitudes of relaxation constants involved in this process.

The theoretical model [103] accounts for the following experimental results of Ref. [12]:

(1) the existence of bursts of moderate and bright fluorescence on the temporal scale of seconds;

(2) the alternation, on the temporal scale of seconds, of dark off-intervals with two types of on-intervals with fluorescence;

(3) the experimentally observed exponential character of on- and off-interval distributions in duration;

(4) the independence of the average off-interval length τ_{off} on the exciting light intensity, and the linear dependence of the average on-interval length τ_{on} on the reciprocal of the excitation intensity.

A quantitative agreement between experimental and calculated data is achieved for the following values of the relaxation constants of the polymer molecule: a conformational change rate of 0.1 s^{-1}, a triplet state lifetime of 0.1 – 0.5 s, an intercombination transition probability of $10^2\ \mathrm{s}^{-1}$ for the transition from the excited singlet state to the triplet state.

The theory elaborated in Ref. [103] makes the following new predictions:

(1) the existence of two types of on-intervals with different fluorescence levels I_1 and I_2, and two types of dark off-intervals which follow the on-intervals with a dim and bright fluorescence I_1 and I_2;

(2) the dependence of the dim – bright fluorescence intensity ratio I_1/I_2 on the signal acquisition interval which was fixed at about 0.1 s in Ref. [12].

An experimental verification of the above predictions and of the significance of the triplet state for conformational changes would substantially advance our understanding of the energy transfer processes in polymer chains.

13. Blinking fluorescence of semiconductor nanocrystals

Quantum dots (QDs) in semiconductors are highly attractive objects on the basis of which efficient lasers can be developed, because they possess narrow fluorescence lines [24]. That is why the electro- and photoluminescence of QDs as well as of semiconductor nanocrystals (NCs) has been much investigated. In the photoluminescence studies of single QDs and NCs, it turned out that some of them exhibit fluorescence fluctuating in intensity, i.e., it is blinking. However, not all QDs or NCs exhibit blinking fluorescence. Among, for instance, InP quantum dots, blinking fluorescence is encountered in one dot per million [32]. On the other hand, in CdSe NCs, the fluorescence blinker is encountered significantly more frequently [27–31].

The fluorescence flicker signifies that the temporal on-intervals, during which the fluorescence exhibits appreciable intensity, alternate with off-intervals, when the fluorescence is completely absent or low in intensity. The flicker is rather simply explained in the case of a single molecule — even for so complex a molecule as a polymer. However, in an NC there are many absorbers and emitters. Why does their fluorescence flicker and what is the character of the on- and off-distributions in QDs and semiconductor nanocrystals?

The question of why the fluorescence of a single CdSe QD with a ZnS shell flickers was first posed nine years ago [23]. At the same time, the problem of blinking QD fluorescence was theoretically explained on the basis of the model involving the Auger ionization of the QD with subsequent neutralization [107]. Although this model provided an explanation for the fluorescence flicker of such a polyatomic object as a QD, it predicted an exponential distribution in duration of the time intervals with and without fluorescence (of the on- and off-intervals). It is precisely this kind of on- and off-interval distributions that is commonly observed in the fluorescence of single molecules.

However, even in the first investigations of the blinking fluorescence of QDs and nanocrystals [23, 27] it was noted that the on- and off-interval distributions proved to be manifestly nonexponential. That is why the off-interval distribution measured by Kuno et al. [28] five years ago in the fluorescence of CdSe NCs, which obeys the $t^{-1.6}$ power law, came to be an evident challenge to the theory. Subsequent research showed that the power character of the off-interval distribution is inherent not only in CdSe NCs, but in CdTe [31] and CdS [34] nanocrystals as well. Porous silicon NCs were also found to exhibit blinking fluorescence with a $1/t^{2.2}$ power distribution law for the on-intervals, and $1/t^{1.3}$ for the off-intervals [108, 109].

The most surprising fact was that the on-interval distribution measured in Refs [29, 31] for CdSe NCs was also described by a law close to $t^{-1.6}$, like the off-interval distribution. This suggested an idea to the authors of Ref. [29] that there exists some universal cause for the manifestation of the power law with this exponent in the on- and off-interval distribution functions. More recently [110, 111], the author of the present review came up with a simple physical model within the framework of which it is possible to provide a reasonable explanation for the power-law statistics of the on-interval distribution measured for CdSe NCs in Refs [29, 31].

13.1 Model for blinking fluorescence

The presently adopted model of the blinking fluorescence of a single CdSe NC wrapped up in the wide-gap ZnS semiconductor is based on the ionization and subsequent neutralization of such an NC as a result of jumps occurring throughout the period of continuous laser irradiation of the NC. According to this model, free electron–hole (EH) pairs, which lose energy and transform into excitons, are constantly produced in the NC under the action of laser light. Since the Bohr radius of a free exciton, which is equal to several nanometers, is comparable to or exceeds the NC dimension, the wave function of this exciton fills the entire NC [25]. In the presence of at least two excitons in the NC there occurs Auger ionization of the NC, whereby the energy of one vanishing exciton is spent on electron (hole) injection into the shell material, where the electron (hole) falls into a trap. In the ionized state, the NC cannot radiate and the glow dies out. The existence of a positive charge in an NC, which was a multiple of one or two electron charges, was experimentally discovered [112, 113]. Some time later, the electron leaves the trap to find itself in the NC again. The nanocrystal becomes neutral, and the fluorescence is restored.

The power off-interval distribution law prompts us that there exists a broad distribution of relaxation times of the above traps, i.e., of the relaxation rates $g_k = 1/\tau_k$, where k is the trap number. As shown below, it is really possible to obtain the power off-interval distribution at a proper choice of the trap distribution over the electron relaxation rates. Accounting for power on-interval statistics encounters greater difficulties. The simple and natural assumption that the electron capture rates, when Auger ionization is created in various traps, will be differed is evidently inadequate to explain the powerlike statistics of on-intervals. Qualitatively discussed in Ref. [29] as the possible reason for the power-law on-interval statistics is the thermal vibrational modulation of the barrier that separates the NC and the trap.

In an NC with a power statistics, evidently the excitons or EH pairs which participate in Auger ionization should differ from each other in the rate with which their electrons escape from the NC. This difference is described by the subscript j which indicates the Auger ionization rate $G_j = 1/t_{\mathrm{A}j}$ of a given exciton. Furthermore, we are forced to assume that the rates G_j may differ by several orders of magnitude for different excitons or EH pairs. This assumption is impossible to comprehend if one relies on the conventional notion of an exciton as a bound EH pair whose wave function is delocalized throughout the NC.

Efros et al. [25] calculated the energy levels and wave functions of excitons in an NC. The s- and p-state eigenfunctions of a spherical potential well were taken for the wave function of an electron and a hole; the NC atoms were assumed to form a perfect crystal. Two of five exciton states are optically passive. It is precisely this model of fluorescent excitons that underlies the Efros–Rosen model which predicts the exponential on-interval statistics.

The Efros–Rosen model [107] operates with the exciton wave function delocalized over the entire NC, and the states of no other type emerge in this model. However, the NC has a boundary, and therefore the NC atoms located at the boundary interact with the shell atoms and with each other

differently, which should give rise to surface energy levels in the NC. To these levels there corresponds an EH-pair wave function localized in the NC subsurface layer. The energy of these localized EH pairs is located above the NC-delocalized exciton band, and therefore these states most likely do not take an active part in luminescence. However, they can play a role of paramount importance in Auger ionization, i.e., affect the on-interval distribution. If the NC is represented by a sphere, the wave function of the surface states will be localized in a narrow spherical layer adjacent to the NC boundary on the inside. Since the atoms of two different semiconductors are contiguous at their interface, there also exists a nonideality of the electronic system of the atoms along the surface of the above spherical layer. Consequently, the atoms of the layer, described by different angles θ and φ of the spherical coordinate system with the origin at the center of the NC, may also differ from each other due to their local environment. That is why the collective state of the spherical layer will break up into several states localized at different points in the layer. The electron – hole pairs localized in subsurface layers with different radii and at different points of these layers will be numbered by a subscript j, and the rate of Auger ionization with the participation of such a localized EH pair will be denoted by G_j.

The above-considered NC model may be described by the following system of balance equations

$$\begin{aligned} \dot{P}_j &= -\left(\frac{1}{T_1}+G_j\right)P_j + LP_0\,,\\ \dot{P}_0 &= \frac{P_j}{T_1} - LP_0 + \sum_k g_k P_{jk}\,,\\ \dot{P}_{jk} &= -g_k P_{jk} + G_{jk} P_j\,. \end{aligned} \tag{129}$$

Here, P_0 is the probability of finding an EH pair in an NC, P_j is the probability of finding, in addition to this pair, the jth electron which will subsequently find itself in some trap, and P_{jk} is the probability of finding an electron in the kth trap upon EH decay via the jth channel, along with the NC devoid of EH pairs. Clearly, G_{jk} is the probability of the jth EH-pair decay with its electron making its way into the kth trap, and g_k is the electron escape probability for the kth trap. It is also evident that P_0 and P_j describe the states of a neutral NC in the presence of fluorescence, i.e., the probability that the NC is in the on-state, while P_{jk} describe the ionized NC states in the absence of fluorescence, i.e., the probability that the NC is in the off-state.

From simple physical considerations it follows that the probabilities of an NC residence in the on- and off-states should tend to zero as the duration of residence tends to infinity. Therefore, they cannot be determined from the system of equations (129), because it follows from Eqns (129) that the probabilities satisfying this system of equation are related by a conservation law

$$P_0 + P_j + \sum_k P_{jk} = 1\,.$$

System (129) governs the dynamics of the QD ionization – neutralization reversible process and permits the calculation of, for instance, the fluorescence AF $g^{(2)}(t)$. The equations for $P_j^{\rm on} = P_j + P_0$ and $P_k^{\rm off} = \sum_j P_{jk}$ can easily be found with the aid of the system of equations (129) in the following way.

On-states. To derive the equations for the on-state distribution function requires discarding in Eqns (129) the term which describes the off-to-on state transition, i.e., the term $\sum_k g_k P_{jk}$. Then, the first two equations, which contain the fluorescent state populations, decouple from the rest and the on-state distribution function can be found from these two equations

$$\begin{aligned} \dot{P}_j &= -\left(\frac{1}{T_1}+G_j\right)P_j + LP_0\,,\\ \dot{P}_0 &= \frac{P_j}{T_1} - LP_0\,. \end{aligned} \tag{130}$$

Clearly, $P_j^{\rm on} = P_0 + P_j$ is the probability of residence in the on-state with the possibility that this state decays via the jth channel. Since $LT_1 \ll 1$, we may put $\dot{P}_j = 0$ in the case when only the slow dynamics is of interest. In this approximation, we find from the first equation of system (130) that

$$P_j = \frac{LT_1}{1+G_jT_1}\,P_0\,. \tag{131}$$

We add up the equations of system (130) to obtain

$$\dot{P}_j^{\rm on} = -L_j\,P_j^{\rm on}\,, \tag{132}$$

where L_j is the rate of on-state decay via the jth channel, and

$$L_j = L\,\frac{\Gamma_j T_1}{1+\Gamma_j T_1 + LT_1}\,. \tag{133}$$

By summation over all $N_{\rm A}$ NC ionization channels, we arrive at the following expression for the on-interval distribution function

$$w_{\rm on}(t) = \frac{1}{N_{\rm A}}\sum_{j=1}^{N_{\rm A}} L_j \exp\left(-L_j t\right). \tag{134}$$

The experimental data of Refs [29, 31] testify to the fact that EH pairs with different ionization times ranging by three orders of magnitude may exist in a CdSe NC.

Off-states. Derivation of the equations for the off-state distribution function requires neglecting in system of equations (129) the term which describes the on-to-off state transition, i.e., the term $G_{jk}P_j$. Then, the third equation of system (129) is independent of the first two, and the off-state distribution function can be found from the equation

$$\dot{P}_{jk} = -g_k P_{jk}\,. \tag{135}$$

By solving this equation we find the expression for the probability $P_k^{\rm off} = \sum_{j=1}^{N_{\rm A}} P_{jk}$ that the system is revealed itself in the ionized state as a consequence of an electron arriving at the kth trap, and the expression for the function describing the off-interval distribution in duration:

$$w_k^{\rm off} = g_k \exp\left(-g_k t\right). \tag{136}$$

The distribution function for the off-intervals of the entire NC, provided that an electron is in some trap, assumes the form

$$w_{\rm off}(t) = \frac{1}{N_t}\sum_{k=1}^{N_t} g_k \exp\left(-g_k t\right), \tag{137}$$

where N_t is the total number of traps in the ionization of the NC. The experimental results of Refs [29, 30] testify that traps

with ionization times differing by three – five orders of magnitude may exist in a CdSe NC.

13.2 Physical on-interval model

By moving from summation to integration in formula (134), we obtain the following expression

$$w_{\text{on}}(t) = \int_{j_1}^{j_2} L(j) \exp\left[-L(j)t\right] N_{\text{on}}(j)\, \mathrm{d}j. \qquad (138)$$

Here, N_{on} describes the distribution of the probabilities of observing light-excited localized excitons in an NC. Since the distribution of the rates L_j spans several orders of magnitude, the rate is expediently taken in the form

$$L(j) = L_0 10^{-j}. \qquad (139)$$

The variable j may be expressed in terms of the spherical layer radius r:

$$j = j_1 + a(r_0 - r), \quad j_2 = j_1 + ar_0, \quad L_0 = L_{\max} 10^{j_1}. \qquad (140)$$

Upon this change, expression (138) assumes the form

$$w_{\text{on}}(t) = \int_0^{r_0} L(r) \exp\left(-L(r)t\right) N_{\text{on}}(r)\, \mathrm{d}r = \int_0^1 L(x) \exp\left(-L(x)t\right) N_{\text{on}}(x)\, \mathrm{d}x, \qquad (141)$$

where $x = r/r_0$ is the dimensionless radius, and

$$L(x) = L_{\min}\left(\frac{L_{\max}}{L_{\min}}\right)^x, \qquad (142)$$

$$L_{\min} = L_0 10^{-j_2}, \quad L_{\max} = L_0 10^{-j_1}.$$

Let us consider an NC as a sphere of radius r_0, and the variable r as the radial variable of an atom in the spherical layer of the NC. Then, it follows from formula (142) that the electrons located at the periphery of the NC possess the highest Auger ionization rate. Figure 20a depicts the distribution function $N_{\text{on}}(x) = 3x^2$ (curve *3*). It corresponds to the case where localized EH pairs, which are responsible for the Auger ionization, are evenly distributed over the NC. Also shown are two functions N_{on} corresponding to the distribution of ionizable EH pairs primarily in the subsurface spherical layer of the NC (curves *1* and *2*). In Fig. 20b, solid lines *1*, *2*, and *3* represent the results of calculations by formulas (141) and (142) with functions *1*, *2*, and *3* plotted in Fig. 20a. It is easily seen that the calculated functions descend by the $1/t^{1+m}$ law with $m = 0.7$, 0.5, and 0.2 for curves *1*, *2*, and *3*, respectively. If we take the function $N_{\text{on}}(x) = 3x^2$, the on-interval distribution function will decrease with an exponent of -1.2 throughout a time interval spanning eight orders of magnitude. However, for a stronger localization of the ionizable excitons near the surface we obtain the laws $1/t^{1.7}$ and $1/t^{1.5}$. The higher the degree of exciton localization, the steeper the decrease in the on-interval distribution function. Calculations indicate that the distribution function $N_{\text{on}}(x) \propto L(x)^m$ substituted into formula (141) yields the distribution function $w_{\text{on}}(t) \propto t^{-(1+m)}$ throughout a time interval spanning n orders of magnitude provided that

$$\log \frac{L_{\max}}{L_{\min}} = j_2 - j_1 > n. \qquad (143)$$

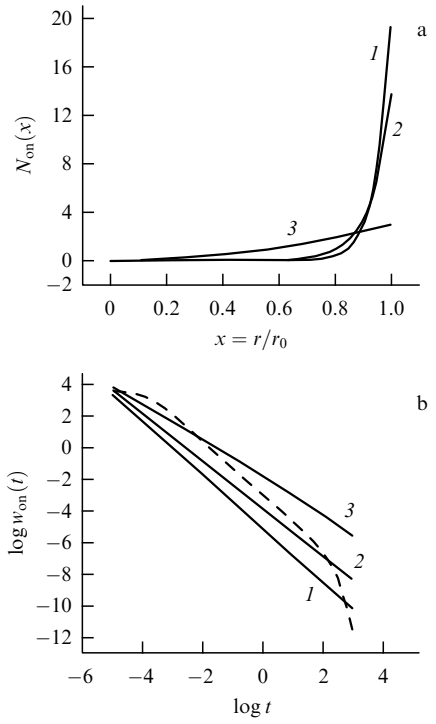

Figure 20. Three distribution functions $N_{\text{on}}(x)$ (a) and their corresponding on-interval distribution functions (b) calculated by formulas (141) and (142) for $L_{\max} = 10^7$ s^{-1}, $L_{\min} = 10^{-5}$ s^{-1} (solid curves *1–3*) and $L_{\max} = 10^4$ s^{-1}, $L_{\min} = 10^{-3}$ s^{-1} (dashed line) [106].

Condition (143) signifies that the time interval between the shortest $(1/L_{\max})$ and longest $(1/L_{\min})$ ionization times exceeds the time interval used in experiment. Solid curve *1* and the dashed curve in Fig. 20b pertain to the same distribution function described by curve *1* in Fig. 20a. The dashed curve in Fig. 20b, which was calculated by formulas (141) and (142) with violation of condition (143), demonstrates what results from the violation of condition (143).

Figure 21 displays the experimental on-interval distribution data for the fluorescence of a CdSe NC with a ZnS shell [31] and the calculated results [110, 111]. In the calculation, use was made of a probability density similar to that depicted in Fig. 20a with different $N(x)$ function build-up rates. From Fig. 21 it follows that the on-interval distribution is close to the $t^{-1.6}$ power law and yet essentially dependent on the excitation intensity and the temperature. It also follows from Fig. 21 that a satisfactory agreement with experiment is possible to achieve by assuming that the probability of finding localized excitons participating in ionization process is higher at the periphery of the NC than at its center.

The temperature dependence of the on-interval distribution is most likely an indication that the Auger ionization mechanism is not the only one. Nirmal et al. [23] and Kuno et al. [28] have advanced arguments for thermal ionization. In a real NC, both mechanisms are supposedly involved. A consideration of the kinetic equations for an NC with the inclusion of the thermal ionization mechanism also leads to formulas (134) and (137), but the ionization constant L_j will depend on the temperature in this case.

13.3 Off-interval model

In CdSe [24, 27 – 29, 31], CdTe [31], and CdS [34] NCs, the off-interval statistics were investigated more extensively than the

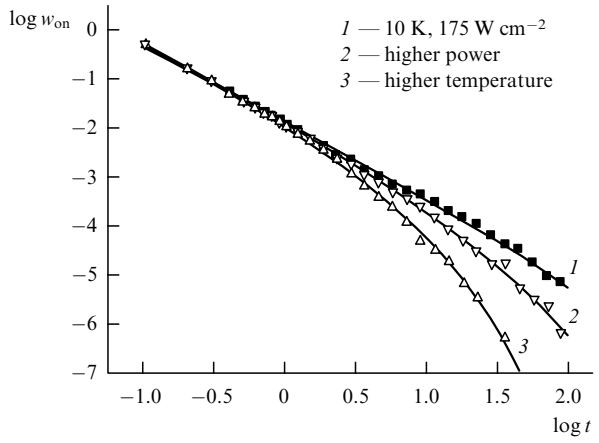

Figure 21. On-interval distribution in a CdSe NC with a ZnS shell under different physical conditions [31]. The solid curves correspond to the calculation by formula (143) with $L_{\min} = 10^{-2}\ \mathrm{s}^{-1}$ and $L_{\max} = 10^{3}\ \mathrm{s}^{-1}$, and different functions $N_{\mathrm{on}}(x)$.

on-interval statistics. The off-interval distribution was found to obey the $1/t^{1+m}$ law, with m ranging from 0.5 to 0.7. The validity range of this power-law statistics amounts to five orders of magnitude on the time scale. It was also verified that the physical factors responsible for the bend of the curves in Fig. 21 do not change the off-interval distribution power law. Let us find under what physical conditions the power-law off-interval statistics may manifest themselves.

Clearly, formula (137) for the off-interval distribution function can be brought to the form

$$w_{\mathrm{off}}(t) = \int_{k_1}^{k_2} \gamma(k) \exp\left(-\gamma(k)t\right) n(k)\, \mathrm{d}k\,, \qquad (144)$$

where $n(k)$ is the function of the density of states integrally normalized to unity. We will find the form of the functions $\gamma(k)$ and $n(k)$ which are responsible for the power distribution law. We assume that the traps are located in the shell material. Since $\gamma(k)$ is the kth-trap neutralization rate, which may range by several orders of magnitude according to experimental data, we will take this function in the form $\gamma(k) = \gamma_0 \exp(-\lambda) = \gamma_0 10^{-k}$, i.e., accept the tunnel neutralization mechanism. The lower λ is, the higher the transmittance of the potential barrier which separates the trap and the QD. Clearly, $\gamma_{\max} = \gamma_0 10^{-k_1}$ and $\gamma_{\min} = \gamma_0 10^{-k_2}$. These formulas suggest that the traps located near the NC surface possess the highest electron escape rate. It is also evident that the majority of traps are resided in the part of the shell adjacent to the NC boundary, i.e., the closer to the NC boundary, the greater the number of traps. Considering the aforesaid about the dependence of the trap deactivation rate on how close the trap is to the NC boundary, the last statement relating to the number of traps can be mathematically written down as

$$n(k) = A_m \gamma^m(k)\,, \qquad (145)$$

where A_m is the normalization factor. Numerical calculation shows that the integration of expression (144) with this probability density yields a power-form distribution

$$w_{\mathrm{off}}(t) \propto t^{-(1+m)} \qquad (146)$$

provided uniquely that the interval $(1/\gamma_{\max}, 1/\gamma_{\min})$ exceeds the time interval in which the off-interval distribution function is investigated.

14. Conclusions

The end of the past century and the beginning of this century saw a rapid development of nanotechnologies, which will inevitably bring about an intensive advancement of the physics of ultrafine particles in the near future. In this case, no realm of solid-state physics will be untouched. Even now there is a wealth of papers concerned with the study of dielectric, semiconductor, and metal nanoparticles. Specific features are immanent in nanoparticle physics because nanoparticles exhibit new properties which are not inherent in bulk materials, and this opens up new vistas for technologies. It is well know, for instance, that a macroscopic metal sample does not fluoresce; moreover, it is a 'quencher' of the fluorescence of organic molecules located on its surface. However, when the macroscopic metal sample is reduced to a nano-sized one, fluorescence must occur, because a single metal atom fluoresces. The question of what the number of metal atoms is whereby a nanoparticle acquires or loses metal properties is among those that still remain open. It is evident that a small number of interacting atoms or molecules may be treated as a quasimolecule irrespective of whether these atoms, when combined in a macroscopic sample, make up a metal, a semiconductor, or a dielectric. That is why the physics of nanoparticles may be termed nanophysics. Nanophysics is significantly different from the physics of macroscopic objects by the nature of the problems under discussion. In the present review, this has been shown and discussed at length by the example of the fluorescence of single molecules and semiconductor nanocrystals.

In nanophysics, specific problems also arise in the comparison of theory and experiment. The interrelation of theory and experiment in nanophysics, which is schematically diagrammed in Fig. 1, has been comprehensively discussed in this review. However, not only do the new problems make their appearance in nanophysics, but also new possibilities for gathering physical information open up. This has been demonstrated in our review, in which the key words are a *single nanoparticle* and *fluorescence fluctuations*. Hopefully, I have managed to show that fluctuating fluorescence can serve as a radically new information source for the construction of physical models both for complex molecules like a polymer molecule and for semiconductor nanocrystals.

Not all experimental results that deserve discussion have been considered in the present review — far from it. I have enlarged on only those experimental results which could be theoretically processed. That is why I discussed only the papers in which the physical information was gained with the aid of fluorescence photons, for the theory of single nanoparticle fluorescence has already been adequately developed. Left beyond the scope of the review was actually the entire nanomicroscopy which makes use of scanning tunnel microscopes, atomic-force microscopes, and scanning near-field microscopes in its investigations. The number of papers in this area is enormous and is increasing in an avalanche-like manner. However, their inherent feature is the prevalence of qualitative discussions of experimental results and a nearly complete absence of theory. This is the reason why this body of papers remained outside the scope of the present review.

This work was supported by the Russian Foundation for Basic Research (grant No. 04-02-17024).

References

1. Dagenais M, Mandel L *Phys. Rev. A* **18** 2217 (1978)
2. Nagourney W, Sandberg J, Dehmelt H *Phys. Rev. Lett.* **56** 2797 (1986)
3. Cook R J, Kimble H J *Phys. Rev. Lett.* **54** 1023 (1985)
4. Plenio M B, Knight P L *Rev. Mod. Phys.* **70** 101 (1998)
5. Moerner W E, Kador L *Phys. Rev. Lett.* **62** 2535 (1989)
6. Orrit M, Bernard J *Phys. Rev. Lett.* **65** 2716 (1990)
7. Moerner W E, Basche Th *Angew. Chem.* **32** 457 (1993)
8. Basché Th et al. (Eds) *Single Molecule Optical Detection, Imaging and Spectroscopy* (Münich: Wiley-VCH, 1997)
9. Moerner W E, Orrit M *Science* **283** 1670 (1999)
10. Osad'ko I S *Opt. Spektrosk.* **89** 749 (2000) [*Opt. Spectrosc.* **89** 690 (2000)]
11. Osad'ko I S *Selektivnaya Spektroskopiya Odinochnykh Molekul* (Selective Spectroscopy of Single Molecules) (Moscow: Fizmatlit, 2000) [Translated into English (Berlin: Springer-Verlag, 2002)]
12. van den Bout D A et al. *Science* **277** 1074 (1997)
13. Ha T et al. *Chem. Phys. Lett.* **271** 1 (1997)
14. Lu H P, Xie X S *Nature* **385** 143 (1997)
15. Dickson R M et al. *Nature* **388** 355 (1997)
16. Lu H P, Xun L, Xie X S *Science* **282** 1877 (1998)
17. Hu D, Yu J, Barbara P F *J. Am. Chem. Soc.* **121** 6936 (1999)
18. van Oijen A M et al. *Science* **285** 400 (1999)
19. Gensch T et al. *Angew. Chem. Int. Ed.* **38** 3752 (1999)
20. Weiss S *Science* **283** 1676 (1999)
21. Yu J, Hu D, Barbara P F *Science* **289** 1327 (2000)
22. Hofkens J et al. *J. Am. Chem. Soc.* **122** 9278 (2000)
23. Nirmal M et al. *Nature* **383** 802 (1996)
24. Gammon D et al. *Science* **273** 87 (1996)
25. Efros Al L et al. *Phys. Rev. B* **54** 4843 (1996)
26. Pistol M-E et al. *Phys. Rev. B* **59** 10725 (1999)
27. Banin U et al. *J. Chem. Phys.* **110** 1195 (1999)
28. Kuno M et al. *J. Chem. Phys.* **112** 3117 (2000)
29. Kuno M et al. *J. Chem. Phys.* **115** 1028 (2001)
30. Sugisaki M et al. *Phys. Status Solidi B* **224** 67 (2001)
31. Shimizu K T et al. *Phys. Rev. B* **63** 205316 (2001)
32. Sugisaki M et al. *Jpn. J. Appl. Phys.* **41** 958 (2002)
33. Shimizu K T et al. *Phys. Rev. Lett.* **89** 117401 (2002)
34. Verberk R, van Oijen A M, Orrit M *Phys. Rev. B* **66** 233202 (2002)
35. Ambrose W P, Basché Th, Moerner W E *J. Chem. Phys.* **95** 7150 (1991)
36. Moerner W E et al. *J. Phys. Chem.* **98** 7382 (1994)
37. Anderson P W, Halperin B I, Varma C *Philos. Mag.* **25** 1 (1972)
38. Phillips W A *J. Low Temp.* **13** 351 (1972)
39. Boiron A-M et al. *Chem. Phys.* **247** 119 (1999)
40. Vainer Yu G et al. *Opt. Spektrosk.* **94** 926 (2003) [*Opt. Spectrosc.* **94** 864 (2003)]
41. Mandel L, Wolf E *Optical Coherence and Quantum Optics* (Cambridge: Cambridge Univ. Press, 1995) [Translated into Russian (Moscow: Fizmatlit, 2000)]
42. Mandel L *Opt. Lett.* **4** 205 (1979)
43. Mandel L *Proc. Phys. Soc. London* **72** 1037 (1958)
44. Kelley P L, Kleiner W H *Phys. Rev.* **136** A316 (1964)
45. Kim M S, Knight P L *Phys. Rev. A* **36** 5265 (1987)
46. Barkai E, Jung Y J, Silbey R *Phys. Rev. Lett.* **87** 207403 (2001)
47. Jung Y, Barkai E, Silbey R J *Adv. Chem. Phys.* **123** 199 (2002)
48. Kim M S, Knight P L, Wodkiewicz K *Opt. Commun.* **62** 385 (1987)
49. Osad'ko I S *Zh. Eksp. Teor. Fiz.* **113** 1606 (1998) [*JETP* **86** 875 (1998)]
50. Basché Th et al. *Phys. Rev. Lett.* **69** 1516 (1992)
51. Mollow B R *Phys. Rev. A* **12** 1919 (1975)
52. Osad'ko I S *Zh. Eksp. Teor. Fiz.* **98** 1045 (1990) [*Sov. Phys. JETP* **71** 583 (1990)]
53. Zheng Y, Brown F L H *Phys. Rev. Lett.* **90** 238305 (2003)
54. Zheng Y, Brown F L H *J. Chem. Phys.* **119** 11814 (2003)
55. Osad'ko I S *Zh. Eksp. Teor. Fiz.* **128** 77 (2005) [*JETP* **101** 64 (2005)]
56. Short R, Mandel L *Phys. Rev. Lett.* **51** 384 (1983)
57. Osad'ko I S, Yershova L B *J. Lumin.* **86** 211 (2000)
58. Verberk R, Orrit M *J. Chem. Phys.* **119** 2214 (2003)
59. Zaitsev N N, Osad'ko I S *Zh. Eksp. Teor. Fiz.* **104** 4042 (1993) [*JETP* **77** 950 (1993)]
60. Donskoi D V, Zaitsev N N, Osad'ko I S *Chem. Phys.* **176** 135 (1993)
61. Osad'ko I S *Zh. Eksp. Teor. Fiz.* **109** 805 (1996) [*JETP* **82** 434 (1996)]
62. Osad'ko I S *Zh. Eksp. Teor. Fiz.* **116** 962 (1999) [*JETP* **89** 513 (1999)]
63. Osad'ko I S, Yershova L B *J. Chem. Phys.* **112** 9645 (2000)
64. Osad'ko I S, Yershova L B *J. Lumin.* **87–89** 184 (2000)
65. Kilin S Ya et al. *Phys. Rev. A* **57** 1400 (1998)
66. Dalibard J, Castin Y, Mølmer K *Phys. Rev. Lett.* **68** 580 (1992)
67. Geva E, Skinner J L *J. Phys. Chem. B* **101** 8920 (1997)
68. Geva E, Skinner J L *J. Chem. Phys.* **109** 4920 (1998)
69. Plakhotnik T *J. Lumin.* **83–84** 221 (1999)
70. Makarov D E, Metiu H *J. Chem. Phys.* **115** 5989 (2001)
71. Dum R, Zoller P, Ritsch H *Phys. Rev. A* **45** 4879 (1992)
72. Wang J, Wolynes P *J. Chem. Phys.* **110** 4812 (1999)
73. Cao J *Chem. Phys. Lett.* **327** 38 (2000)
74. Gardiner C W, Parkins A S, Zoller P *Phys. Rev. A* **46** 4363 (1992)
75. Reynaud S *Ann. Phys.* (Paris) **8** 315 (1983)
76. Barsegov V, Chernyak V, Mukamel S *J. Chem. Phys.* **116** 4240 (2002)
77. Barkai E, Silbey R, Zumofen G *Phys. Rev. Lett.* **84** 5339 (2000)
78. Naumov A V et al. *Phys. Rev. B* **63** 212302 (2001)
79. Maier H et al. *Phys. Rev. Lett.* **74** 5252 (1995)
80. Osad'ko I S, Lobanov A N *Opt. Spektrosk.* **99** 306 (2005) [*Opt. Spectrosc.* **99** 289 (2005)]
81. Osad'ko I S, in *Spectroscopy and Excitation Dynamics of Condensed Molecular Systems* (Modern Problems in Condensed Matter Sciences, Vol. 4, Eds V M Agranovich, R M Hochstrasser) (Amsterdam: North-Holland, 1983)
82. Osad'ko I S *Phys. Rep.* **206** 43 (1991)
83. Gladenkova S N, Osad'ko I S *Chem. Phys. Lett.* **187** 628 (1991)
84. Vainer Yu G et al. *J. Chem. Phys.* **116** 8959 (2002)
85. Anderson P W *J. Phys. Soc. Jpn.* **9** 316 (1954)
86. Klauder J R, Anderson P W *Phys. Rev.* **125** 912 (1962)
87. Reinecke T L *Solid State Commun.* **32** 1103 (1979)
88. Bai Y S, Fayer M D *Phys. Rev. B* **39** 11066 (1989)
89. Reilly P D, Skinner J L *J. Chem. Phys.* **101** 959, 965 (1994)
90. Osad'ko I S, Khots E V *Single Mol.* **3** 236 (2002)
91. Osad'ko I S, Khots E V *Opt. Spektrosk.* **94** 949 (2003) [*Opt. Spectrosc.* **94** 885 (2003)]
92. Osad'ko I S *Zh. Eksp. Teor. Fiz.* **120** 991 (2001) [*JETP* **93** 865 (2001)]
93. Osad'ko I S, Yershova L B *J. Chem. Phys.* **111** 7652 (1999)
94. Zilker S J, Haarer D *Chem. Phys.* **220** 167 (1997)
95. Hannig G et al. *Mol. Cryst. Liq. Cryst.* **291** 11 (1996)
96. Tchenio P, Myers A B, Moerner W E *J. Lumin.* **56** 1 (1993)
97. Fleury L et al. *J. Lumin.* **56** 15 (1993)
98. Kozankiewicz B, Bernard J, Orrit M *J. Chem. Phys.* **101** 9377 (1994)
99. Naumov A V et al. *J. Chem. Phys.* **116** 8132 (2002)
100. Vainer Yu G et al. *Opt. Spektrosk.* **94** 936 (2003) [*Opt. Spectrosc.* **94** 873 (2003)]
101. Vainer Yu G et al. *J. Lumin.* **107** 287 (2004)
102. Mirzov O et al. *Chem. Phys. Lett.* **386** 286 (2004)
103. Osad'ko I S *Zh. Eksp. Teor. Fiz.* **123** 696 (2003) [*JETP* **96** 617 (2003)]
104. Harrison N T et al. *Phys. Rev. B* **53** 15815 (1996)
105. Swager T M, Gil C J, Wrighton M S *J. Phys. Chem.* **99** 4886 (1995)
106. Osad'ko I S, Chigirev A R *Fiz. Tverd. Tela* **23** 538 (1981)
107. Efros Al L, Rosen M *Phys. Rev. Lett.* **78** 1110 (1997)
108. Cichos F, Martin J, von Borczyskowski C *Phys. Rev. B* **70** 115314 (2004)
109. Cichos F, Martin J, von Borczyskowski C *J. Lumin.* **107** 160 (2004)
110. Osad'ko I S *Pis'ma Zh. Eksp. Teor. Fiz.* **79** 522 (2004) [*JETP Lett.* **79** 416 (2004)]
111. Osad'ko I S *Chem. Phys.* **316** 99 (2005)
112. Krauss T D, Brus L E *Phys. Rev. Lett.* **83** 4840 (1999)
113. Krauss T D, O'Brien S, Brus L E *J. Phys. Chem. B* **105** 1725 (2001)